UNIVERSITY
OF MICHIGAN
APR 2 1951
ENGINEERING
LIBRARY

THE AERONAUTICAL QUARTERLY

Volume II FEBRUARY 1951. Part IV

CONTENTS

Supersonic Flow Investigations with a "Hydraulic Analogy" Water Channel — *Joseph Black* and *O. P. Mediratta*

Contracting Ducts of Finite Length — *L. G. Whitehead*, *L. Y. Wu* and *M. H. L. Waters*

The Properties of Crossed Flexure Pivots and the Influence of the Point at which the strips cross — *W. H. Wittrick*

An Analysis of the Lift on Straight, Yawed and Swept-back Wings — *J. Lockwood Taylor*

LONDON
ROYAL AERONAUTICAL SOCIETY
4 HAMILTON PLACE W1

10/-

THE AERONAUTICAL QUARTERLY

Editorial Board

W. G. A. PERRING, C.B., F.R.Ae.S. (*Chairman*)

Dr. H. ROXBEE COX, D.I.C., F.R.Ae.S., F.I.Ae.S.

Professor S. GOLDSTEIN, F.R.S., F.R.Ae.S.

Sir GEOFFREY TAYLOR, F.R.S.

G. H. DOWTY, F.R.Ae.S. (Chairman of the JOURNAL Committee of the Royal Aeronautical Society)

J. SMITH, C.B.E., F.R.Ae.S., A.M.I.Mech.E. (Chairman of the Technical Board and Executive Committee of the Society of British Aircraft Constructors)

Joint Editors

Capt. J. Laurence Pritchard, C.B.E., Hon.F.R.Ae.S., Hon. F.I.Ae.S.
Joan Bradbrooke, A.R.Ae.S.

Editorial Referees

Aerodynamics

(a) General

Prof. L. BAIRSTOW
Dr. G. P. DOUGLAS
Prof. A. A. HALL
Sir B. MELVILL JONES
Mr. D. KEITH-LUCAS
Dr. N. A. V. PIERCY
Mr. W. G. A. PERRING
Mr. E. F. RELF
Prof. E. J. RICHARDS

(b) Fluid Motion

Mr. A. FAGE
Prof. S. GOLDSTEIN
Prof. L. HOWARTH
Mr. W. P. JONES
Prof. M. J. LIGHTHILL
Dr. J. W. MACCOLL
Dr. J. H. PRESTON
Mr. L. F. G. SIMMONS
Mr. H. B. SQUIRE
Sir GEOFFREY TAYLOR
Prof. G. TEMPLE
Prof. A. D. YOUNG

(c) Stability and Control

Mr. L. W. BRYANT
Mr. S. B. GATES
Mr. G. T. R. HILL
Mr. H. B. IRVING
Mr. G. H. LEE
Mr. M. B. MORGAN

Helicopters and Propellers

Dr. J. A. J. BENNETT
Mr. L. G. FAIRHURST
Mr. R. HAFNER
Capt. R. N. LIPTROT
Mr. J. MULLIN

Instruments and Electrical Equipment

Dr. G. E. BAIRSTO
Mr. G. W. H. GARDNER
Mr. C. S. HUDSON
Mr. A. N. IRENS
Mr. C. N. JAQUES
Mr. F. W. MEREDITH

Aircraft Design

Mr. R. BOORMAN
Mr. R. M. CLARKSON
Mr. A. N. CLIFTON
Mr. W. S. FARREN
Mr. H. H. GARDNER
Mr. H. KNOWLER
Mr. W. E. W. PETTER
Mr. F. H. POLLICUTT
Mr. A. E. RUSSELL
Mr. R. S. STAFFORD

Radio and Radar

Mr. J. F. ATHERTON
Mr. B. G. GATES
Mr. R. L. SMITH ROSE
Dr. A. M. UTTLEY
Sir ROBERT WATSON WATT

Aviation Medicine

Dr. A. BUCHANAN BARBOUR

Meteorology

Prof. D. BRUNT
Mr. J. K. HARDY
Prof. P. A. SHEPPARD

Sound

Mr. N. FLEMING
Mr. W. MAKINSON

Aircraft Propulsion

Mr. H. CONSTANT
Sir A. H. ROY FEDDEN
Dr. S. HOOKER
Mr. A. R. HOWELL
Mr. P. LLOYD
Dr. A. W. MORLEY
Dr. E. S. MOULT
Mr. N. S. MUIR
Mr. F. NIXON
Mr. F. M. OWNER
Dr. D. PYE
Mr. H. SAMMONS
Prof. O. A. SAUNDERS

Air Transport

Mr. P. G. MASEFIELD
Mr. N. E. ROWE
Mr. W. TYE

Aircraft Accessories

Mr. W. C. CLOTHIER
Mr. H. G. CONWAY
Mr. G. H. DOWTY
Mr. R. GRAHAM

Vibration and Flutter

Prof. A. R. COLLAR
Prof. W. J. DUNCAN
Mr. R. A. FRAZER
Dr. A. ROBINSON
Mr. H. TEMPLETON

Performance

Mr. H. DAVIES
Mr. D. R. NEWMAN
Mr. A. H. YATES

Structures

Mr. A. C. BROWN
Mr. H. L. COX
Mr. D. J. FARRAR
Dr. H. ROXBEE COX
Prof. W. S. HEMP
Mr. H. B. HOWARD
Mr. E. D. KEEN
Mr. F. A. KERRY
Dr. D. M. A. LEGGETT
Prof. R. L. LICKLEY
Prof. A. J. SUTTON PIPPARD
Prof. A. G. PUGSLEY
Dr. S. C. REDSHAW
Mr. R. H. SANDIFER
Sir RICHARD SOUTHWELL

Fuels and Oils

Mr. E. L. BASS
Mr. J. W. DRINKWATER
Prof. F. H. GARNER
Prof. W. E. GARNER
Dr. K. E. W. RIDLER
Dr. C. G. WILLIAMS

Materials

Prof. L. AITCHISON
Dr. N. P. ALLEN
Prof. N. F. MOTT
Mr. L. ROTHERHAM
Dr. H. SUTTON
Dr. C. SYKES

Flight Testing

Mr. P. A. HUFTON
Mr. E. T. JONES
Mr. S. SCOTT HALL
Mr. H. L. STEVENS

SUPERSONIC FLOW INVESTIGATIONS WITH A "HYDRAULIC ANALOGY" WATER CHANNEL

by

JOSEPH BLACK, M.Sc., A.F.R.Ae.S.,
and
O. P. MEDIRATTA, M.A., B.Sc.
(*Department of Aeronautical Engineering, University of Bristol*)

SUMMARY

This paper describes the construction of a water channel in the University of Bristol for the investigation of the analogy between the two-dimensional flow of a gas and that of shallow water with a free surface. Both continuous and discontinuous flow were examined, with a view to determining the limitations of the analogy.

Continuous "shooting" water flow was found to be reasonably analogous with supersonic isentropic gas flow, a static depth of about half an inch appearing to be satisfactory with this particular channel. No independent check was made of the agreement, or otherwise, between "streaming" water flow and subsonic gas flow, since the method of checking used was the measurement of the angle of the waves formed on the water surface, and such waves exist only in "shooting" flow.

Quantitative agreement between hydraulic jumps and shock waves was not obtained; this is in accordance with the theoretical predictions given in the text. It was found possible, however, to use hydraulic jumps to simulate qualitatively most of the features of gas flow with shock waves, such as flow in a Laval nozzle, or past a supersonic aerofoil; photographs of these jumps are included in the paper. The most valuable aspect of the water channel undoubtedly lies in the ease with which these phenomena may be demonstrated visually, and its construction for this purpose can be recommended.

Further work of a quantitative nature, especially concerned with mixed flow regimes, is contemplated.

1. INTRODUCTION

The resemblance between the waves formed by a body moving at a supersonic speed through air, and the surface waves produced by a moving ship, or in water

Paper received September 1950.
[The Aeronautical Quarterly, Vol. II, February 1951]

flowing past bridge piers, was first commented on by Mach[1]. It was not until 1920 that the analogy* between two-dimensional gas flow and the flow of water with a free surface was first developed by Jouguet[2], and later by Riabouchinsky[3]. They showed that the mathematical equations governing the two flows were of the same nature if the water were replaced by a fictitious "hydraulic gas" with a ratio of specific heats of 2.0. In 1937, Binnie and Hooker[4] investigated the flow in a channel with a constriction. Preiswerk[5], in his application of the methods of gas dynamics to the accurate determination of the water flow in a converging-diverging channel, provided a very complete account of the analogy; since he was primarily interested in the water flow as such, and not in its possible application to gas flow, his work is of limited value for the purposes of this paper. Attempts to confirm Riabouchinsky's work by quantitative measurements of lift and drag in streaming (subsonic) flow were made in 1939[6], and investigation of the flow through a cascade of turbine blades by this method was made in 1942[7].

The National Advisory Committee for Aeronautics have had a water channel in operation for some time, the first investigation reported[8] being a comparison with the subsonic flow about a circular cylinder. A later paper[9] reviews the practical details of the operation of this water channel, and gives some comments on the design of water channels in general. An examination of the corresponding flow of water and air in a number of cases has been made in Italy[10], and work has also been in progress in the California Institute of Technology; using a different type of apparatus, the emphasis there is on the relations between hydraulic jumps and shock waves[11].

In view of the comparative simplicity of the apparatus, and the promising results obtained by previous investigators it was decided to construct a small water channel, one of the objects being to determine the limitations of the method.

Notation

a	velocity of sound
c	velocity of surface wave propagation
C_p	specific heat at constant pressure
d	water depth
F	Froude number, $V/(gd)^{\frac{1}{2}}$
M	Mach number, V/a
p	pressure
T	absolute temperature
u	velocity component along x-axis

*A brief account of the analogy is given in Appendix I.

v velocity component along y-axis

V velocity

γ ratio of specific heats, C_p/C_v

λ wavelength

ρ density

σ surface tension

Suffix 0 denotes reservoir conditions.

Suffix 1 denotes conditions in front of the shock or jump.

Suffix 2 denotes conditions behind the shock or jump.

2. DESCRIPTION OF THE APPARATUS

2.1. *The water channel*

For ease of construction the channel was made inside a standard galvanised steel trough 5 feet by 18 inches, and 15 inches deep (Figs. 1 and 2). The bed of the channel consisted of a horizontal sheet of clear plate glass $\frac{1}{4}$ inch thick, the water being led up to it over a convex dam of copper sheet. From the sump, the water was returned to the reservoir by a small centrifugal pump driven by a $\frac{1}{2}$ h.p. D.C. motor. To lessen the surging and turbulence, the water entered the reservoir through a tube of fine mesh gauze which extended across the tank; this tube in turn was shielded by a curved sheet, and additional gauzes were inserted across the reservoir.

Two methods were employed to accelerate the water over the bed; one was a converging-diverging nozzle, and the other a sluice gate. In the first, designed primarily for studying the flow through nozzles, there was a fixed contraction of varnished mahogany, which brought the width down from 18 inches to just over 2 inches at the throat. Attached to the wooden contraction, and extending downstream from the throat, were two vertical walls of 2-inch stainless steel strip; the nozzle profile over this section could be altered rapidly by push-pull rods pivoted to the strip. Movement of these rods was effected by means of screwed rods which passed through gimbals in the tank walls.

This method had the disadvantage that the stream at exit from the nozzle had only a maximum width of about 4 inches, which was too narrow for the study of flow patterns around bodies in the stream. As an alternative, therefore, the fixed contraction together with the adjustable walls was removed, and a sluice gate, which could be raised or lowered to give a variable width slit at the bottom, was fitted across the upstream end of the bed (Fig. 1(*b*)). After passing under the sluice, the stream was contained between two vertical walls which ran the length of the bed; these walls were diverged slightly to allow for boundary layer thickening.

With both methods a simulation of back pressure could be made by raising an adjustable dam from the sump so that it projected above the downstream edge of the bed, and thus blocked the flow.

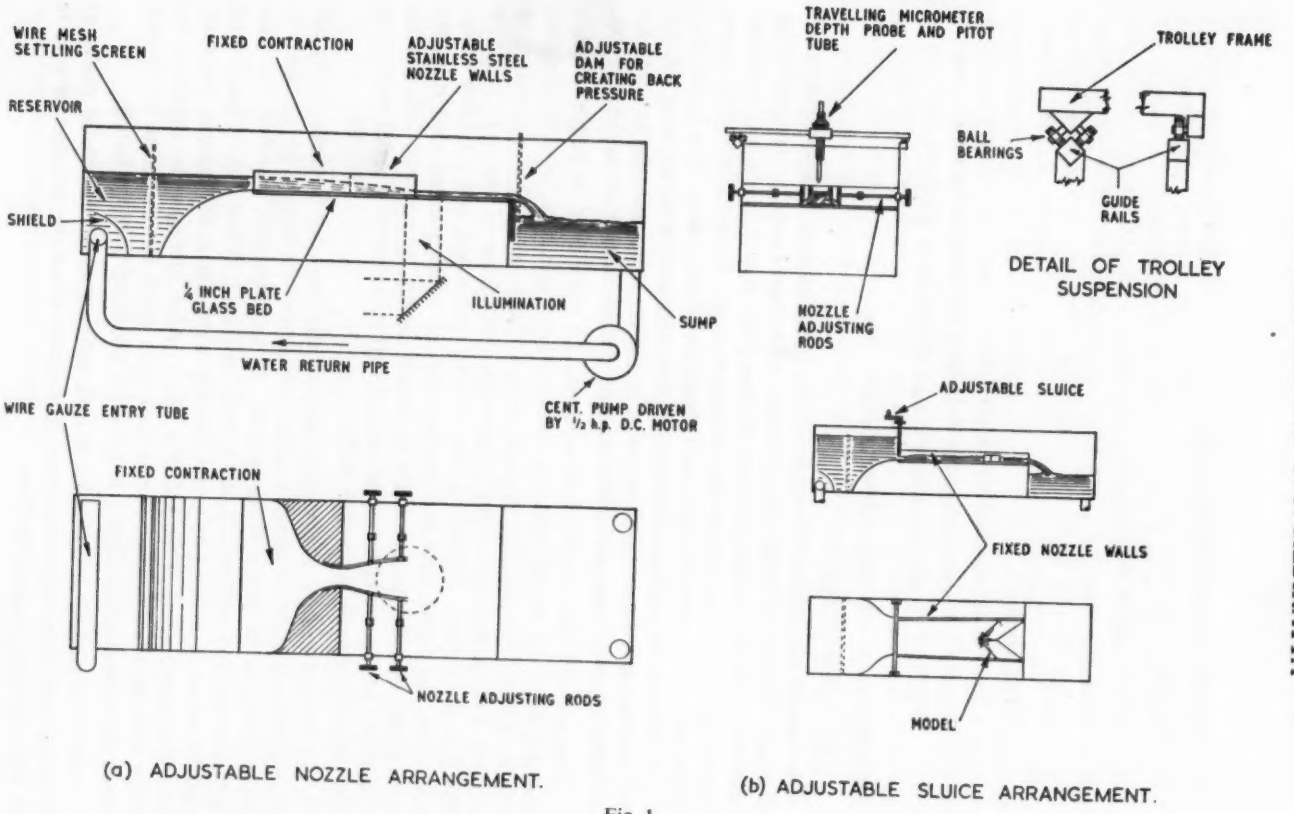

Fig. 1.
Diagrammatic sketch of water channel.

Diagrammatic sketch of water channel.

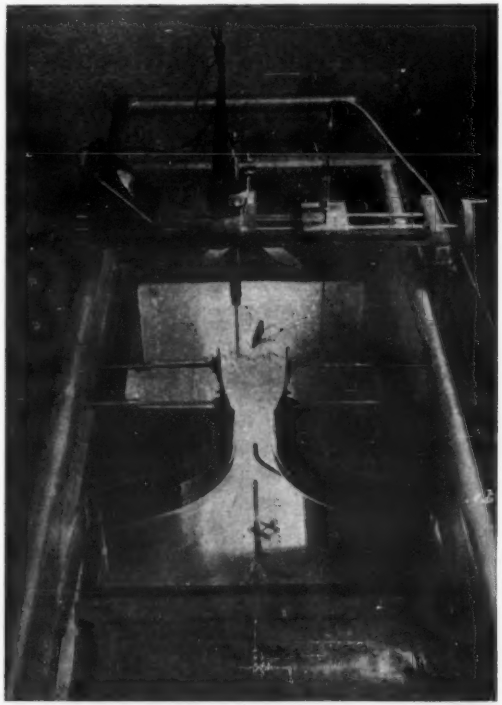

Fig. 2(*a*).
View of channel looking downstream.

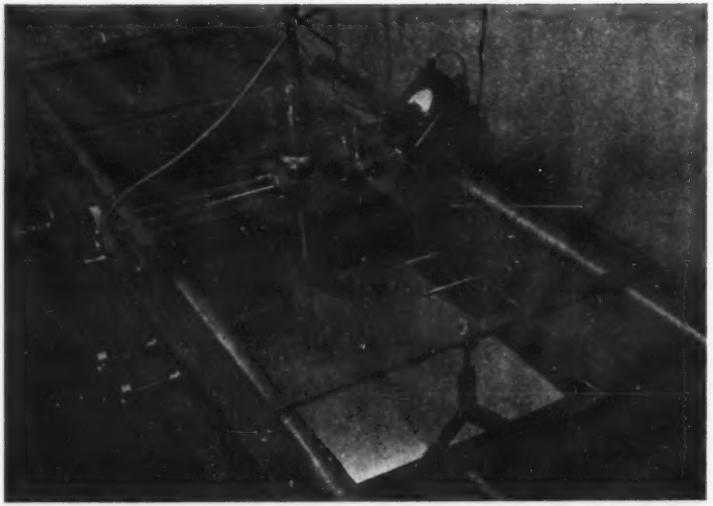

Fig. 2(*b*).
View of channel looking upstream.

In order to diminish the effects of capillarity, which play no part in the analogy, the water in the tank had 0.05 per cent. Teepol added to it. This approximately halves the surface tension.

2.2. *Measuring apparatus*

Water depths at any point in the field of flow could be measured accurately to ± 0.002 inch with a micrometer depth gauge carrying a probe. This gauge was mounted on a block which could be traversed along a trolley by means of a micrometer-screwed rod (Fig. 2). The trolley in turn could travel the length of the tank; the position of the gauge in the flow field could be accurately determined from vernier scales on the trolley, and along the trolley guide rails.

These guide rails of selected one-inch square brass were attached to, and ran horizontally the length of, the tank walls, one being mounted with a surface horizontal, and the other with surfaces at 45° (Fig. 1). A single point of support on one side of the trolley was provided by a small ball-bearing attached vertically to the trolley and running along the horizontal-surface guide rail. The other two points of support on the opposite side also provided the lateral restraint; they each consisted of a pair of small ball-bearings mounted opposite each other on the trolley at 45°, so that they ran along the top inclined surfaces of the other guide rail. A spacing of 6 inches between the two pairs was found to give sufficient restraint.

Deflection of an electrostatic voltmeter, mounted in series with the survey probe, gave a positive indication of its contact with the water surface. This was of particular value upstream of the throat, and in regions of flow where the capillary waves formed by the probe tip on contact with the surface are difficult to detect visually. For the investigation of boundary layers and velocity distributions, pitot and static tubes made of hypodermic tubing, and mounted on a similar depth gauge, were used. Pressure measurements from these tubes were made on a Chattock three-liquid type micro-manometer*.

2.3 *Photographic technique*

Various lighting systems had to be used to suit differing types of flow. In general the flow was illuminated from directly below with a parallel beam shining through a large rectangular aperture cut in the bottom of the tank. For some cases the surface itself was photographed, while in others it was the shadow of the flow cast on to a ground glass screen above the surface which was recorded.

For recording surface wave angles which were propagated along the length of the nozzle, a strip of 60 mm. recording paper was held in contact with the under surface of the glass bed, and a photo-flood bulb about 4 feet above the water surface was flashed on and off.

See Appendix II.

3. INVESTIGATION OF CONTINUOUS (SHOCKLESS) FLOW

3.1 *Analogy relations*

The analogy may be summarised as follows*:

Two-Dimensional Gas Flow	*Water Flow (Hydraulic Gas)*
Density ratio ρ/ρ_0	Water depth ratio d/d_0
Temperature ratio T/T_0	Water depth ratio d/d_0
Pressure ratio p/p_0	(Water depth ratio)^2, $(d/d_0)^2$
Velocity of sound, $a, = (\gamma p/\rho)^{\frac{1}{2}}$	Wave Velocity, $(gd)^{\frac{1}{2}}$
Mach number $M, = V/a$	Froude number $F, = V/(gd)^{\frac{1}{2}} = [2(d_0 - d)/d]^{\frac{1}{2}}$
Subsonic Flow	Streaming Water
Supersonic Flow	Shooting Water

From the expressions for analogous pressure and density relations, it will be seen that the ratio of specific heats in the "hydraulic gas" must be 2.0 (Equation (12), Appendix I), whereas in air, for example, it is 1.4. This difference does not limit the method. In the water channel experiments an attempt is made to get agreement between the measured values of the water depths and those calculated by gas-dynamic theory for the "hydraulic gas," and not those calculated for a real gas. If such an agreement can be obtained, then by further calculation using the appropriate values of γ the hydraulic gas results can be converted to those of a real gas.

It is very important to understand clearly the significance of the Froude number as here defined. In general, the Froude number is the non-dimensional quantity $V/(gl)^{\frac{1}{2}}$, where V is the velocity of flow of the liquid at a representative point, g is the acceleration due to gravity, and l is any representative length. The particular velocity and length which will be used in this work is the local velocity and the local depth, so that the Froude number throughout this paper refers to the quantity $V/(gd)^{\frac{1}{2}}$.

First consider the velocity of flow V. From equation (6) in Appendix I, it is given by $[2g(d_0 - d)]^{\frac{1}{2}}$, where d_0 is the depth of water in the reservoir and d is the local depth. This relation can be checked by direct measurement of the velocity with pitot-static tubes and comparison with the appropriate depth measurements.

The quantity $(gd)^{\frac{1}{2}}$ is of a more complex nature. It is actually the velocity of propagation of gravity waves on the water surface for conditions where the depth d is small compared to the wavelength λ (equation (14) of Appendix I); if these conditions do not exist the propagation velocity includes a further term, and $(gd)^{\frac{1}{2}}$ has no longer this particular significance.

*See Appendix I.

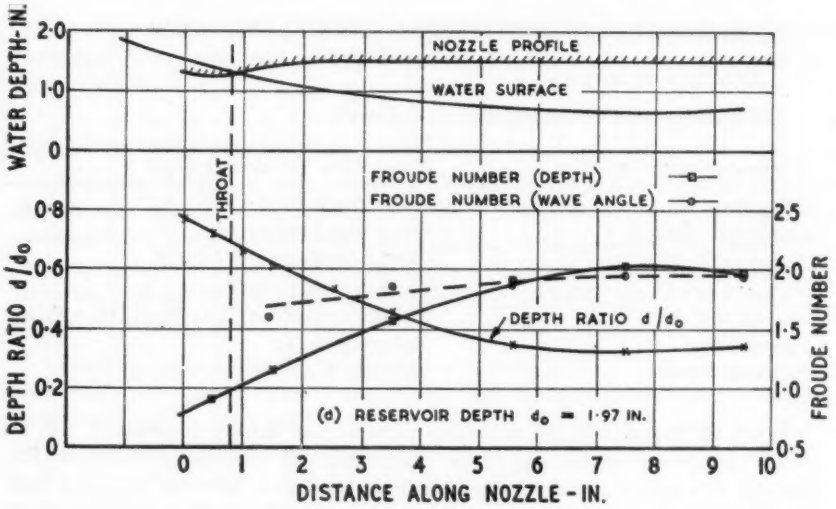

Fig. 4(*a*).
Water flow along a converging-diverging nozzle ($d_0 = 1.97$ in.).

In shallow water flow, therefore, where theoretically the depth d is small compared to the wavelength λ, the Froude number as defined above is the ratio of the local velocity of flow to the local velocity of propagation of gravity waves on the water surface. As such it is thus directly comparable to the local Mach number in a gas flow, which is the ratio of the local velocity of flow to the local velocity of propagation of sound waves. It must be stressed that it is only the Froude number defined as $V/(gd)^{\frac{1}{2}}$ in the stipulated conditions, and no other, which can be regarded as comparable to the Mach number.

In previous investigations[5, 8] the Froude number in the form $[2(d_0 - d)/d]^{\frac{1}{2}}$ was used for the determination of the optimum depth of water to be employed. The depth d at the point where the Froude number F is unity will be $\frac{2}{3}$ of the reservoir depth d_0; if it is assumed that F is unity at the throat of the channel then the depth there should be $\frac{2}{3}\ d_0$. Accordingly, the depths in the water channels were adjusted until they satisfied this assumed condition, and these depths were then quoted as the ones to be used.

The objection to this procedure is that in itself it does not reveal whether the defined Froude number does in fact represent the ratio of flow velocity to wave propagation velocity. In other words, it does not check experimentally whether the flow conditions are such that the wave propagation velocity is accurately given by $(gd)^{\frac{1}{2}}$. Such a check, however, can be made.

A point source of disturbance in a shooting flow of water will propagate surface waves, and the angle which the envelope of these waves makes with the direction of

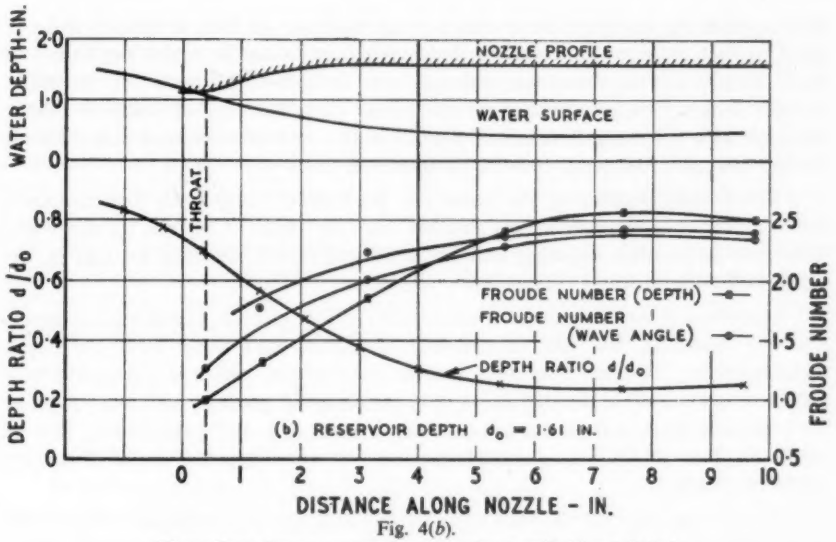

Fig. 4(*b*).
Water flow along a converging-diverging nozzle ($d_o = 1.61$ in.).

flow will have the value $\sin^{-1}(1/F)$ only if the depth conditions are as postulated in the analogy. Measurement of this angle thus provides a simple experimental check on the optimum depth of the water.

3.2. *Determination of the optimum depth*

The first step in this work was to measure the water depths at a number of stations along the nozzle, downstream of the throat, with the reservoir depth being held constant. A strip of Perspex, through which metal probes projected at right angles, was placed horizontally over the nozzle, so that the probes lay along its centre-line; the probes were then pushed down until their tips just touched the surface at approximately the same intervals as the original depth measurements. The surface waves were then recorded on recording paper held under the channel bed. Measurements of depths and photographs were repeated independently for each condition examined. In addition, pitot-static pressure traverses were made at the same locations in some cases.

The wave angles on the recording paper (Fig. 3, *see* page 241) had to be carefully assessed. In order to attain the maximum reliability, the wave angles from the two sets of photographs were measured independently by two observers, before the Froude number had been calculated from the depth measurements.

Typical results are shown in Figs. 4(*a*) and 4(*b*). It will be seen that at the downstream end of the nozzle the agreement between the Froude number as determined by the wave angle, and that from depth measurements, is reasonably

good considering the order of accuracy of the method. In fact, it appears to be as good as that obtained in a comparable experiment in air[12], where the values of Mach numbers from wave measurements were thought to be good only to within ± 3 per cent. This agreement was maintained over the range of reservoir depths available with this channel, that is, 1.6 to 2.1 inches. Results obtained with different profiles also gave the same measure of agreement.

The Froude number at the throat as determined from depth measurements, which naturally is the only means possible since no "Mach" wave is formed there, was found to be unity, agreeing with the results of earlier investigators, that is, the depth in the throat was $\frac{2}{3}$ of that in the reservoir.

Immediately downstream of the throat the values given by wave measurements are very scattered, but are all consistently higher than those from the depth measurements. This point requires further investigation, which is impossible with the existing channel; a channel is required which could produce a flow at outlet at least one inch deep, at the same values of depth ratios d/d_0 as in these cases. Results from this flow might then indicate whether the non-agreement arises from the increased depth.

Part of the discrepancy may arise from deficiencies in technique. When the wave angles are large, as they are for small Froude numbers, for example, about 40° at $F=1.5$, it becomes increasingly difficult to distinguish them from the curved capillary waves. In addition, the slope of the water surface, which may be seen in Fig. 4 to have become appreciable, would introduce a further error, since the recording method is essentially a shadowgraph of the surface. It is possible also that the expression for the wave propagation velocity, which is developed on the assumption that the wave is being propagated along a horizontal surface, requires modification when the wave is actually being propagated on a sloping surface, as in this case.

Measurements of the velocity of flow with vertical pitot-static traverses indicated a uniform velocity profile above the boundary layer, the thickness of which at the end of the nozzle was of the order of 0.1 inch with a water depth of 0.5 inch. The velocity measured above the boundary layer agreed with that calculated from the depth measurements.

These results would seem to indicate that for a water depth of about $\frac{1}{2}$ inch the Froude number determined from the expression $[2(d_0-d)/d]^{\frac{1}{2}}$ may be taken as analogous to the Mach number in isentropic gas flow. This depth, however, should not be regarded as the only one to give good agreement; theoretical work still in progress appears to indicate that the flow need not necessarily be so shallow. The advantage of being able to use a greater depth is that the boundary layer is likely to be a proportionally smaller part of the measured depth. In designing a new water channel, therefore, a depth of about one inch should be allowed for, if possible; application of the technique already outlined will rapidly determine the optimum depth for the particular channel.

The N.A.C.A. investigation on flow past cylinders[8] was made at depths which were claimed to be equivalent to subsonic Mach numbers; this implies an acceptance of the depth relation for the Froude number in a region where no independent check similar to that already described can be made, since wave forms of the type examined do not exist in streaming flow. One feature of their results is the different flow patterns created by the same body at the same "Mach" number, for depths varying from ½ to 2 inches (Figs. 13 and 14 of Ref. 8). By comparing these patterns with that produced by a cylinder in a high speed wind tunnel the agreement is found to be best for a static water depth between 0.75 and 1.0 inch. Interpretation of flow patterns in streaming flow should be made with extreme care, however, since there is a type of wave formation which can occur in such conditions, and to which there is no analogy in air[13, 14]. These waves are being examined further.

4. INVESTIGATION OF DISCONTINUOUS FLOW

4.1. Shock waves and hydraulic jumps

In the flow of either a gas or water, it is possible for a discontinuity to exist. With a gas, the phenomenon is the shock wave, passage through which causes an abrupt rise in the pressure, density, and temperature of the gas, and a decrease in the velocity. In the case of water flow, the discontinuity manifests itself as a sudden rise in the depth, which is termed the "hydraulic jump"[15]. A common example of such a jump is the circular one formed in the spread of a jet of water impacting on a horizontal surface (Fig. 5, *see* page 241)*.

It is interesting to compare these phenomena, and hence examine the extent to which they may be regarded as analogous to each other. For simplicity, only jumps and waves normal to the flow will be examined.

Water: The hydraulic jump can only occur in shooting water, the flow being reduced to streaming conditions behind it. Eddies are produced on the face of the jump (Fig. 6), and therefore there is a loss in what might be termed the "mechanical" energy of flow (the total energy of course remains constant, the eddying creating heat which cannot be re-utilised in liquid flow).

The flow through the jump is governed by the following equations.

Continuity: $$V_1 d_1 = V_2 d_2, \quad . \quad . \quad . \quad . \quad . \quad (1)$$

Momentum: $$\tfrac{1}{2} g d_1^2 + d_1 V_1^2 = \tfrac{1}{2} g d_2^2 + d_2 V_2^2, \quad . \quad . \quad . \quad . \quad (2)$$

*Another type of hydraulic jump, in which the rise occurs in an undulating, rather than an abrupt, manner, can also be formed. It is not discussed here, because it arises only if the depth ratio is below 2.0, and such conditions were not examined. In any case, no theoretical explanation of the undulating hydraulic jump has yet been given.

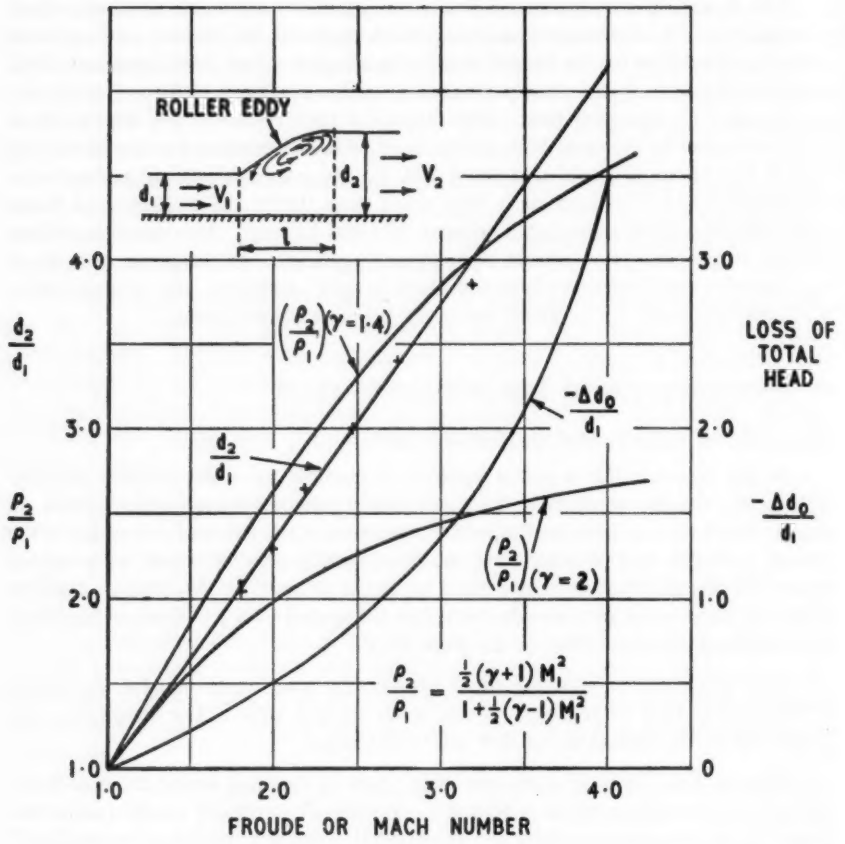

Fig. 6.
Flow relations across a shock wave and a hydraulic jump.

Energy: $$d_1+V_1^2/(2g)=d_2+V_2^2/(2g)+h=d_0, \quad . \quad . \quad . \quad (3)$$

where h represents the eddying losses in the jump.

The "mechanical" energy of the flow is the sum of the pressure energy and kinetic energy, and is measured by the total head pressure represented by d_0. Fig. 6 shows how the loss in total head Δd_0 through a jump increases with Froude number; for example, if the jump is formed at an F of 3.0 the loss in total head is about 1.3 times the depth of water in front of the jump. From these equations it is possible by expressing V in terms of d and the Froude number in front of the jump

to show that the depth ratio d_2/d_1 is a function of the Froude number alone. The expression is

$$d_2/d_1=\tfrac{1}{2}\left[(1+8F^2)^{\frac{1}{2}}-1\right]. \quad . \quad . \quad . \quad . \quad . \quad (4)$$

The relation between d_2/d_1 and F is plotted in Fig. 6. Measurements of d_2/d_1 from the jumps formed in this channel are also plotted; the agreement is excellent. Similar results were obtained by Bakhmeteff[15], and confirm equation (4).

Gas: A shock wave can only be formed in a gas flowing at supersonic velocity. The equations governing its propagation are

Continuity: $$\rho_1 V_1=\rho_2 V_2, \quad . \quad . \quad . \quad . \quad . \quad . \quad (5)$$

Momentum: $$p_1+\rho_1 V_1^2=p_2+\rho_2 V_2^2, \quad . \quad . \quad . \quad . \quad . \quad . \quad (6)$$

Energy: $$\tfrac{1}{2}V_1^2+\frac{\gamma}{\gamma-1}\frac{p_1}{\rho_1}=\tfrac{1}{2}V_2^2+\frac{\gamma}{\gamma-1}\frac{p_2}{\rho_2}=\frac{\gamma}{\gamma-1}\frac{p_0}{\rho_0}=C_p T_0, \quad . \quad (7)$$

Density relation (from Rankine-Hugoniot): $$\frac{\rho_2}{\rho_1}=\frac{\tfrac{1}{2}(\gamma+1)M_1^2}{1+\tfrac{1}{2}(\gamma-1)M_1^2} \quad . \quad (8)$$

The gas flow has pressure and kinetic energy; in addition, it has a third form, which is its internal energy. Comparing the energy equations (equations (3) and (7)) for the jump and shock, it will be seen that in flow through a shock wave there are no losses of a like nature to the eddying loss involved. It is true that there is a loss in the total head pressure in going through the shock wave, and this might appear to be comparable to the same loss in the jump. This is not the case, however, because while the total head pressure d_0 is a measure of the energy of the water flow, it is the total head temperature T_0 which measures the energy of the gas flow. The drop in total head pressure through the shock wave is only an indication of the re-distribution which is taking place between the kinetic, pressure and internal energies of the gas.

Since the energy transport is so different in the two phenomena, it is to be expected that the relations derived and verified for continuous flow, which were based on analogous energy equations, will not apply to the discontinuous flow. It follows that if a hydraulic jump has formed in the water flow, depth measurements downstream of it cannot bear the same simple relation to the gas density as in the continuous case, and the analogy in that form breaks down. It is thus meaningless to put a value of 2.0 for γ in the Rankine-Hugoniot relation, in order to obtain density ratios which will agree with those deduced from the measured depths through a jump.

This lack of agreement may be seen in Fig. 6. If the analogy relations held, the line of d_2/d_1 against F would also represent the density ratio ρ_2/ρ_1 for a shock wave

formed in a "hydraulic gas," where γ was 2.0. The curves obtained by using a γ of 2.0 in the shock wave relation are also plotted, and the divergence between it and the jump depth ratio is apparent.

It should be noted that the values of depth ratio through the jump are for water to which no surface-tension reducing agents were added. Such agents are reported[11] to have a considerable influence on the form of the profile of the hydraulic jump. Ref. 11 also records a lack of agreement between hydraulic jumps and shock waves in air, in an investigation using an apparatus in which jumps were produced by a rapid discharge of water into a shallow layer of static water.

4.2. *Qualitative agreement between shocks and jump*

In spite of the quantitative difference between a shock wave and a hydraulic jump there is a remarkable agreement between their propagation and resulting wave patterns. Some examples of these are discussed.

4.2.1. *Flow through a converging-diverging nozzle*

The behaviour of a gas flow in a converging-diverging nozzle as the receiver to reservoir pressure ratio is steadily reduced, is well known*. When the receiver pressure ratio is only a little below that necessary to produce critical conditions at the throat, a normal shock wave forms across the nozzle slightly downstream of the throat; this wave travels down the nozzle as the receiver pressure drops, until it lies across the nozzle exit.

With further reduction in receiver pressure the normal wave branches into two oblique shock waves which extend into the receiver. These are intersected by a small normal wave, but this disappears as the receiver pressure drops, until only the two oblique waves extending completely across the flow remain. When the design pressure ratio is reached, the flow at exit should be free from any shock waves, although it may still be intersected with Mach waves.

With a decrease of receiver pressure below the design value, the gas at exit is flowing into a region at a lower pressure: consequently the jet expands in the familiar Prandtl-Meyer expansions, that is, through fan-shaped expansions radiating from the corners of the nozzle exit.

In Fig. 7 (*see* page 242) may be seen the effect of decreasing back pressure on the formation of hydraulic jumps in a converging-diverging nozzle. The back pressure was simulated by raising the dam up from the sump. The progress of the jump is identical to that already described for the shock wave. In Fig. 7(*b*) the normal jump has moved downstream from Fig. 7(*a*), and in Figs. 7(*c*) and 7(*d*) the normal intersection between the oblique jumps is well defined. Flow out of the nozzle was not parallel, as it appears in the photographs; the straight edges are those of the illuminating slot below.

*See, for example, Ref. 17.

Fig. 3.
Surface wave angles as recorded on recording paper.

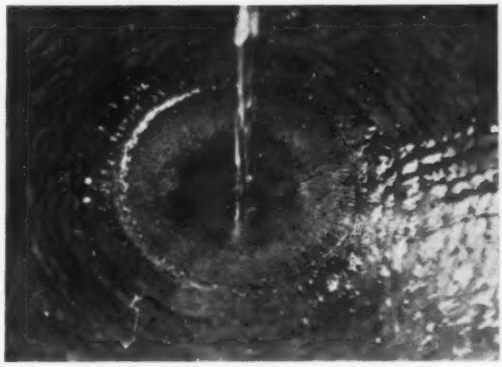

Fig. 5.
Circular hydraulic jump formed in the spread of a jet impacting on a horizontal surface.

Fig. 11.
Channel blockage caused by putting the model at such a large incidence that a second throat has been formed.

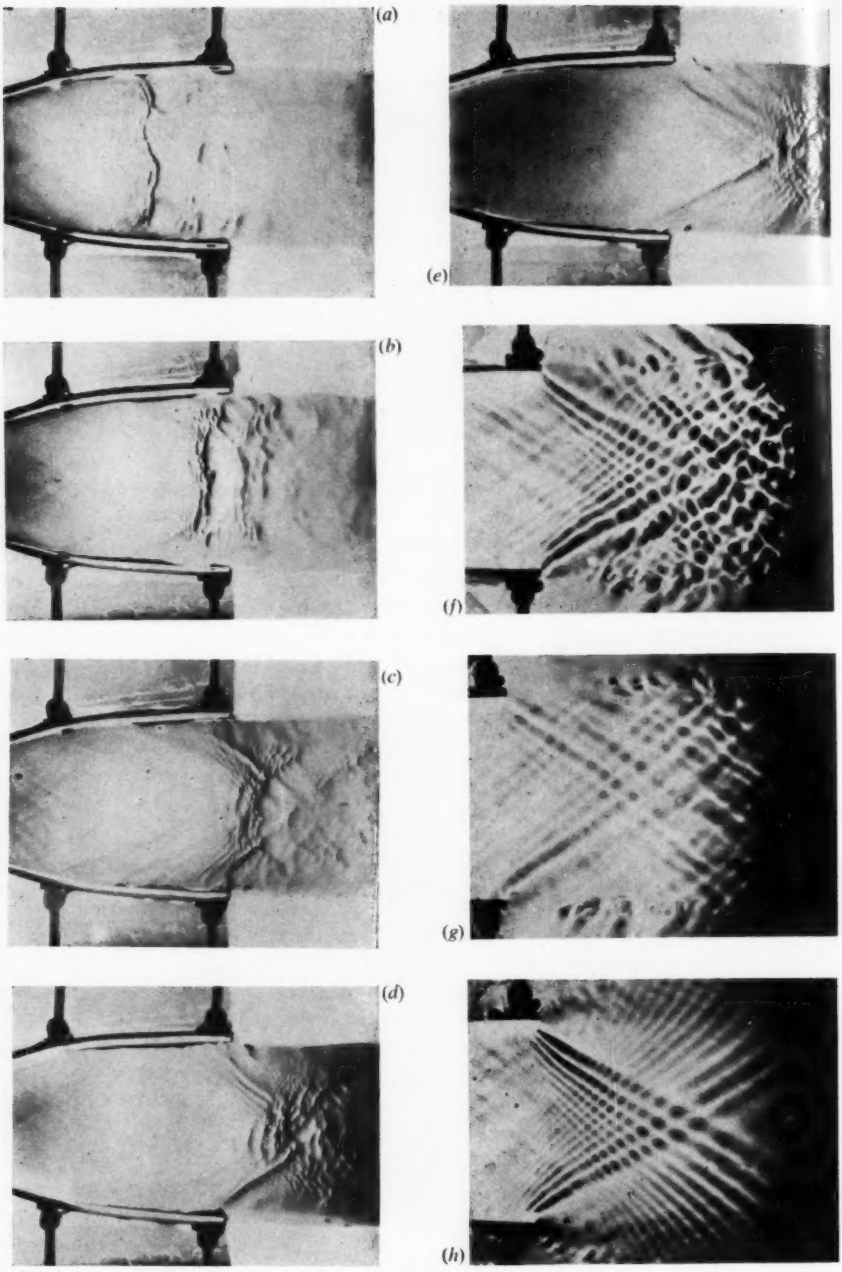

Fig. 7.
Effect of decreasing back pressure on the flow of water in a converging-diverging nozzle.

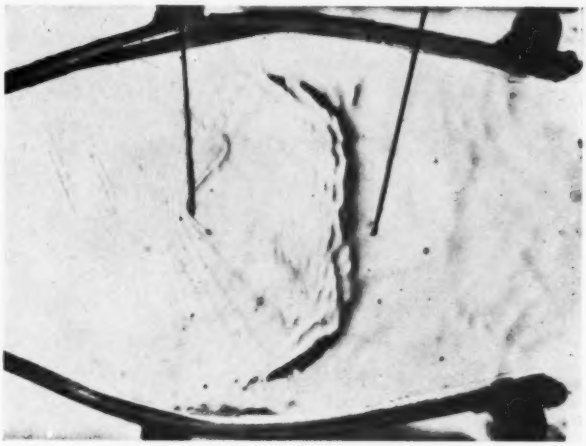

Fig. 8.
The hydraulic jump formed across "shooting" water by a second throat.

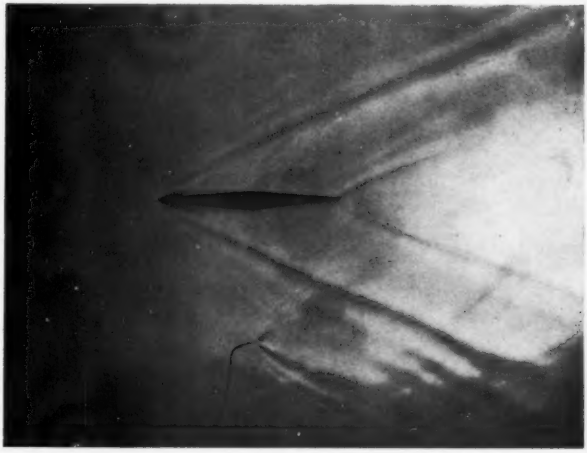

Fig. 9.
Hydraulic jumps formed on a double-wedge aerofoil at zero incidence in a "shooting" stream.

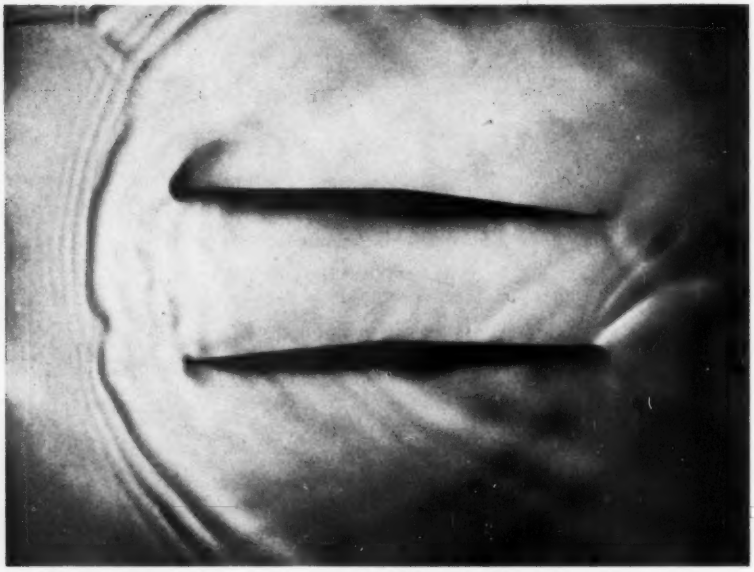

Fig. 10(*a*).
The hydraulic jump formed ahead of a "choked" duct in a "shooting" stream.

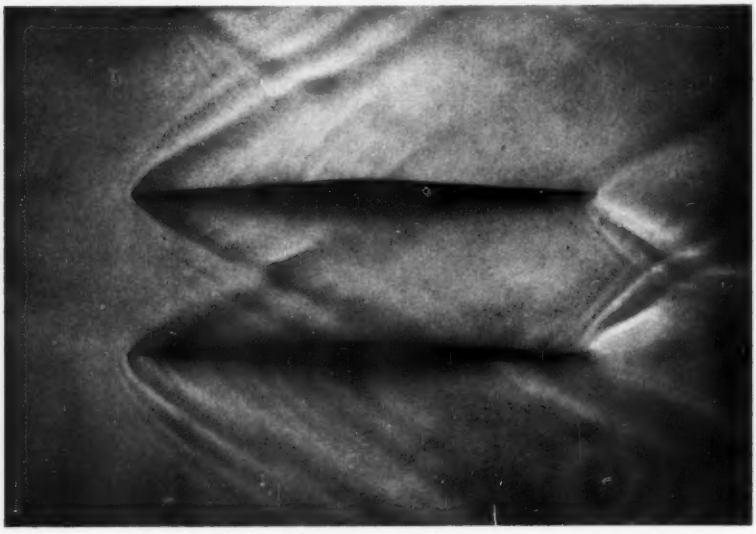

Fig. 10(*b*).
The hydraulic jump system which results when the throat area of the duct in (*a*) is increased to allow the total mass flow to pass.

With the decrease to the back pressure of Fig. 7(*e*), the normal intersection has disappeared. For studying the flow patterns with further reduction of back pressure it was found that shadowgraphs were better than photographs of the water surface. To correlate the two, therefore, a shadowgraph of Fig. 7(*e*) taken with a circular-beam illumination is given in Fig. 7(*f*).

The design back pressure is reached in Fig. 7(*g*), in which there is a parallel jet free from jumps. The Mach waves criss-crossing the flow are clearly visible.

Finally, in Fig. 7(*h*), the expansion of the jet into a region of lower depth is seen. The spreading of the waves from the corners is very pronounced, and the general honeycomb pattern compares almost exactly with those sketched by Courant and Friedrichs[16] for gas flow. There is a remarkable resemblance between the shadowgraph of the water "expansion" and that obtained in an infinite fringe interferogram of an expansion in air[18]. It is interesting to compare Figs. 7(*f*) and 7(*h*), because although the extension of the waves appears identical in both, the former are clearly shock waves, since the waves do not intersect each other without mutual interference. With the expansion, however, the intersection is followed by a smooth and continuous deflection of the waves.

4.2.2. *Convergence of supersonic stream*

A similar effect to that of a high back pressure in the receiver, as already discussed, may be produced by making a supersonic flow converge by means of a second throat. This causes a shock wave to form.

Again this phenomenon can be reproduced in water flow. Fig. 8 (*see* page 243) shows the normal jump formed across the flow ahead of the second throat. The wave formation from the probe tip touching the surface ahead of the wave shows that the water there is shooting, while the absence of such waves behind the jump confirms that the jump reduces the flow to streaming conditions.

4.2.3. *Double-wedge aerofoil*

The jump system around a double-wedge aerofoil at zero incidence is shown in Fig. 9 (page 243). Both the leading and trailing edge shock waves of gas flow are reproduced as jumps, and the Mach waves emanating from the nose surfaces and ending in the leading edge jumps can also be distinguished.

When placed at an incidence greater than the semi-nose angle, the system of shock waves and expansions of gas flow was similarly reproduced, although it is not illustrated here.

4.2.4. *Supersonic diffusers*

An important practical problem is the diffusion of a supersonic gas stream entering a forward-facing intake. This diffusion, which accompanies the reduction

of the stream to subsonic conditions, depends upon the shock wave system existing at the inlet. Two distinct systems can be produced, depending on the amount of convergence of the duct. As a simple picture of what may happen, the duct may be regarded as a reversed Laval nozzle, and therefore there is an exact ratio between the inlet area and the area of the "throat" farther downstream, for any given inlet Mach number.

If the duct converges to a throat area which is below the design value, it cannot swallow all the mass of air which the inlet is capable of passing. There is consequently a "piling-up" of air in front of the inlet and some air will spill over. The shock wave formed in this case will be a bow wave ahead of the intake, thus resembling the wave formed ahead of a blunt-nosed body, although in the latter case the wave would be farther ahead.

When the "throat" area of the duct is large enough, all the mass of air which the inlet can pass will flow through the duct. The result of this new flow condition is that the bow shock wave can move towards the inlet and become attached to the intake lips. The shock system in this case will consist of the oblique shock waves, both internal and external, from the lips. Depending on the Mach number and lip angle, the internal waves may have a normal wave intersection.

Figures 10(*a*) and 10(*b*) (page 244) illustrate this phenomenon with hydraulic jumps. In the first case, the duct is over-converged and an intense jump forms a short distance ahead of the intake. With a larger throat area this jump has moved and attached itself to the lips; the internal oblique jumps from the lips coalesce with a small normal intersection and penetrate each other to reach the opposite walls of the duct.

It should be noted that, while the normal jump ahead of the duct in Fig. 10(*a*) must obviously reduce the flow to streaming conditions, the slight divergence of the duct from the throat to the trailing edge is sufficient to accelerate the flow to shooting conditions again. Thus the features of exit from a Laval nozzle are repeated, namely, two oblique jumps emanating from the trailing edges. Over the external surfaces in Fig. 10(*b*) the wave formation resembles that on the double-wedge aerofoil of Section 4.2.3.

These wave patterns in Fig. 10(*b*) are of interest also as examples of the supersonic biplane as proposed by Busemann.

4.2.5. *Tunnel Blockage*

A problem which can arise in a two-dimensional test in a supersonic wind tunnel is illustrated in Fig. 11 (page 241). When a model is placed in the working section, it effectively divides the section into two channels. With a change of incidence, the "exit" area of the lower channel, formed between the model's trailing edge and the nozzle wall, is reduced. This reduction, if sufficient to choke the

channel, will then cause an almost normal shock wave to form ahead of the "inlet," that is, from ahead of the leading edge across to the nozzle wall. It is thus comparable to the first case of the supersonic diffuser discussed in Section 4.2.4.

In this photograph, the double-wedge aerofoil has been placed at a large incidence in the water channel, and immediately a normal jump has formed from slightly ahead of the leading edge across to the tunnel wall.

The formation of small oblique roots to the normal jumps, which appear in this and other photographs, is probably due to boundary layer effects.

The wave system in the water flow in this case is strikingly identical to that recently photographed in a supersonic wind tunnel[19]; even the oblique root at the interaction of the shock or jump is similar in both cases. While such agreement may be largely fortuitous, it does suggest that further examination of the interaction of hydraulic jumps and boundary layers might be of value.

5. CONCLUSIONS

The water channel provides a convenient analogous flow to the isentropic flow of a gas. Since this type of flow is reasonably completely understood, there is little further knowledge to be gained about it from this apparatus.

In the field where additional information would be welcome, that is, flow with shock waves, the analogy breaks down quantitatively, and it does not yet appear possible to establish any fundamental relation between the flow of gas through a shock wave, and that of water through a hydraulic jump.

Fortunately the qualitative agreement between the phenomena is good, and the water channel is undoubtedly an excellent piece of demonstration apparatus, as the photographs included in the paper confirm. It might be of value, therefore, for indicating the shock wave pattern to be expected in any new system, for example, oblique shock entries for supersonic diffusers.

There remain the serious restrictions that the method only gives an indication about conditions in two-dimensional flow, whereas most practical problems are three-dimensional, and that the boundary layer effects in the gas may differ widely from those in the water.

Further work is contemplated with this water channel; it is hoped to examine the conditions of mixed streaming and shooting flow in order to determine whether transonic investigations are possible.

ACKNOWLEDGMENTS

The authors wish to thank Professor A. R. Collar for his helpful criticisms throughout the investigation, and also the laboratory staff of the Department for their part in the construction of the apparatus.

APPENDIX I

The analogy between water flow with a free surface and two-dimensional compressible gas flow

Consider water flowing along a horizontal plane bottom, bounded by vertical walls and with an upper free surface at constant pressure.

A correspondence is established between the flows of water and gas by examining the continuity, energy, and wave propagation relations for each.

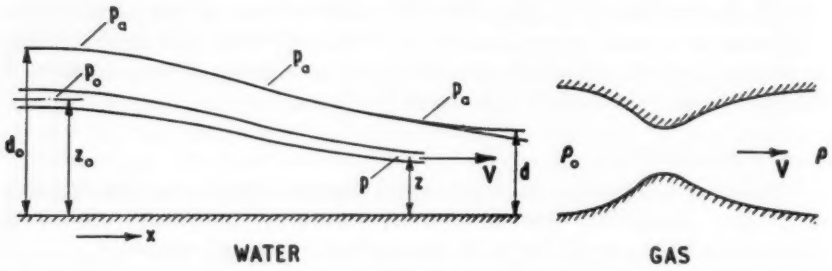

Fig. 12.

(*a*) *Continuity equation*

Water: Assume the vertical acceleration of the water flow to be negligible compared to that of gravity. Let u and v be the velocity components along the x and y co-ordinates, where x and y are measured in the horizontal plane along and normal to the direction of flow. The equation of continuity for two-dimensional flow is

$$\frac{\partial}{\partial x}(du)+\frac{\partial}{\partial y}(dv)=0, \quad . \quad . \quad . \quad . \quad . \quad . \quad (1)$$

where d is the depth.

Gas: For steady two-dimensional gas flow

$$\frac{\partial}{\partial x}(\rho u)+\frac{\partial}{\partial y}(\rho v)=0, \quad . \quad . \quad . \quad . \quad . \quad (2)$$

where ρ is the density.

From (1) and (2) the depth in water flow corresponds to the density in the gas, that is,

$$\rho/\rho_0 \equiv d/d_0 \quad . \quad . \quad . \quad . \quad . \quad (3)$$

(*b*) *Energy equation*

Water: With frictionless flow, Bernoulli's equation for the stream tube shown is

$$p+\tfrac{1}{2}\rho V^2+\rho gz=p_0+\rho gz_0,$$

$$\text{or}\quad V^2=2g(z_0-z)+2(p_0-p)/\rho. \qquad (4)$$

The static pressure at any point in the flow depends only on its depth below the free surface, that is,

$$p_0=\rho g(d_0-z_0)\ \text{and}\ p=\rho g(d-z). \qquad (5)$$

Thus from equations (4) and (5)

$$V^2=2g(d_0-d). \qquad (6)$$

The maximum velocity the flow can attain exists at the point where d is zero,

therefore $$V_{max}^2=2gd_0,$$

hence $$(V/V_{max})^2=(d_0-d)/d_0. \qquad (7)$$

Gas: For gas flow the energy equation is

$$\tfrac{1}{2}V^2+C_pT=C_pT_0=\tfrac{1}{2}V_{max}^2,$$

where T is the absolute temperature and C_p is the specific heat at constant pressure.

Thus $$V^2=2C_p(T_0-T). \qquad (8)$$

and $$(V/V_{max})^2=(T_0-T)/T_0. \qquad (9)$$

From equations (6) and (8), or (7) and (9), it can be seen that the depth ratio in water corresponds to the temperature ratio in the gas, that is,

$$T/T_0\equiv d/d_0. \qquad (10)$$

Equations (3) and (10) give two more relationships. Considering the gas only, it has an equation of state, $p=\rho RT$. Substituting the equivalent density and temperature relations,

$$p/p_0=(\rho/\rho_0)(T/T_0)\equiv(d/d_0)^2 \qquad (11)$$

Thus the square of the depth ratio in the water flow is equivalent to the pressure ratio in the gas.

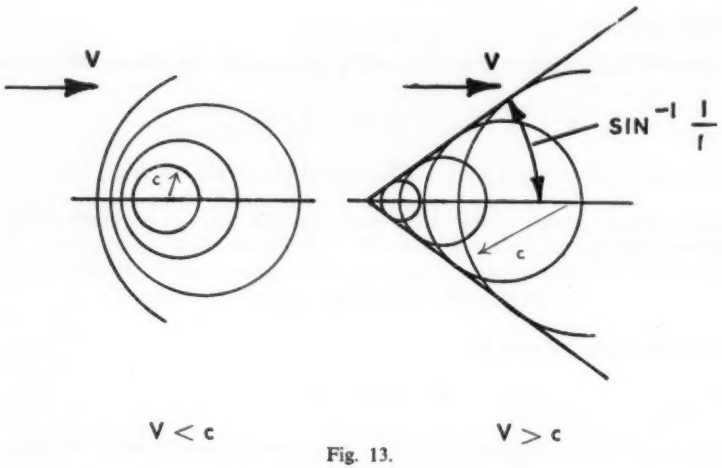

Fig. 13.

Since the isentropic pressure-density relation for a gas is $p=K\rho^{\gamma}$,

$$p/p_0=(\rho/\rho_0)^{\gamma},$$

which from equations (3) and (11) can only be satisfied for a value of

$$\gamma=2. \quad . \quad . \quad . \quad . \quad . \quad . \quad (12)$$

The water flow may thus be regarded, not as directly analogous to a real gas, but to a fictitious "hydraulic gas" (as Jouguet called it) which has a ratio of specific heats of 2.0.

Velocity of wave propagation

Water: In this case interest is centred in the velocity of propagation of gravity waves on the water surface, and not in pressure propagation through the water. In general, the expression for the velocity of propagation of surface waves is

$$c=\left[\left(\frac{\varrho\lambda}{2\pi}+\frac{2\pi\sigma}{\rho\lambda}\right)\tanh\frac{2\pi d}{\lambda}\right]^{\frac{1}{2}}, \quad . \quad . \quad . \quad (13)$$

where λ is the wave length, ρ is the density, σ is the surface tension, and d is the depth[14]. If the depth d is small compared to the wave length λ, the velocity of propagation of the gravity waves becomes

$$c=(gd)^{\frac{1}{2}} \quad . \quad . \quad . \quad . \quad . \quad . \quad (14)$$

The capillary waves, represented by the second term, thus do not in this case play any part in the analogy.

Gas: The analogous wave in this case is a sound wave, which is propagated through the fluid with velocity a, where

$$a=(\gamma p/\rho)^{\frac{1}{2}} \quad . \quad . \quad . \quad . \quad . \quad . \quad (15)$$

Froude number and Mach number

The criterion for the dynamic similarity of the two wave propagations is the ratio of the free stream velocity to the wave propagation velocity. Thus in the case of water, from equations (6) and (14)

$$V/c=V/(gd)^{\frac{1}{2}}=[2(d_0-d)/d]^{\frac{1}{2}}=F, \text{ the Froude number}, \quad . \quad (16)$$

while in a gas,

$$V/a=M, \text{ the Mach number}. \quad . \quad . \quad . \quad . \quad (17)$$

For values of F or M less than one the wave can be propagated in all directions, its propagation velocity upstream of the source being $V-a$, and $V+a$ downstream. With F or M greater than one, however, the wave front is the envelope of the circles, in the case of water, or spheres in a gas, the centres of which are being carried

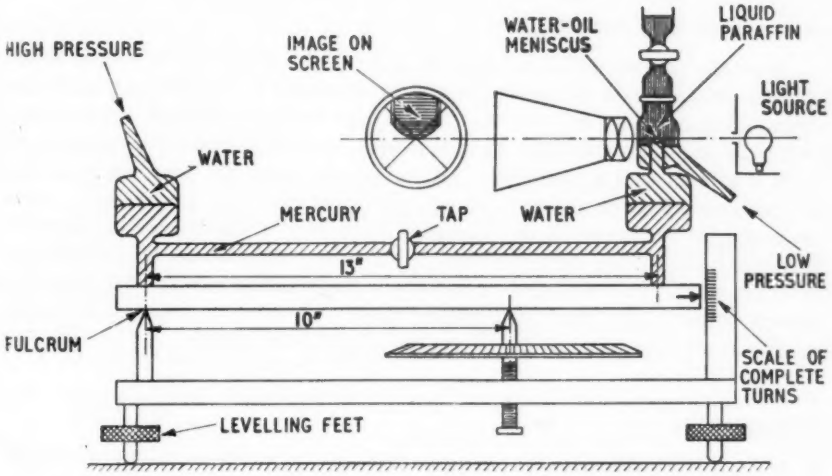

Fig. 14.

Chattock micro-manometer for liquid pressures.

downstream with velocity V. The semi-nose angle of this triangular or conical envelope will be $\sin^{-1}(1/F)$ or $\sin^{-1}(1/M)$.

Thus a water flow with Froude number less than one should correspond to subsonic gas flow, and F greater than one to supersonic gas flow, that is

Mach number or Froude number	*Water*	*Gas*
<1	"Streaming"	Subsonic
>1	"Shooting"	Supersonic

APPENDIX II

Chattock micro-manometer for liquid pressure measurements

This instrument is a development of the more familiar water-oil Chattock micro-manometer for air pressures. The basic principle is that the displacement of a column of mercury in a glass U-tube, caused by the excess pressure in the left-hand bottle (Fig. 14), is compensated for by tilting the whole tube, so that the mercury column is again in equilibrium. An indication of the null point is given by the return of the magnified image of a water-oil meniscus to the intersection of cross-lines on a screen. To form this meniscus, oil is allowed to enter the right-hand bottle from the top until its separates the water in the inner tube above the mercury from that in the bottle. The meniscus observed is the convex one formed on the ground lip of the inner tube.

Since the pressure difference must be equal to the height the right-hand bottle has been raised above the zero setting, it is necessary to measure accurately its vertical displacement. In order to do this, the U-tube is mounted in a frame pivoted at one end, and tilted by means of a vertical screwed rod, rotation of which is effected with a large disc. The height the bottle has been raised is thus easily determined from the amount of rotation of this disc, which has a scale engraved upon its circumference. Complete revolutions of the disc are indicated on the vertical scale at the right-hand end of the base. The number of turns can be converted to pressure difference by a conversion factor taking account of the distance between bottles, screw pitch, and relative density of water to mercury; it is thus possible to measure pressure differences to ± 0.005 inch water.

REFERENCES

1. MACH, E. (1887). Photography of Projectile Phenomena in Air. *Sitzungberichte der Wiener Akademie*, p. 164, Vol. 95, 1887.

2. JOUGUET, E. (1920). Some Problems in General Hydrodynamics. *Journal de Mathématiques Pures et Appliquées* (Series 8), Vol. 3.1., 1920.

3. RIABOUCHINSKY, D. (1932). On the Hydraulic Analogy to Flow of a Compressible Fluid. *Comptes Rendus de l'Academie des Sciences*, p. 998, Vol. 195, 1932.
(1934). Some New Remarks on the Hydraulic Analogy. *Comptes Rendus de l'Academie des Sciences*, p. 632, Vol. 199, 1934.

4. BINNIE, A. M. and HOOKER, S. G. (1937). The Flow under Gravity of an Incompressible and Inviscid Fluid through a Constriction in a Horizontal Channel. *Proc. Roy. Soc.*, p. 592, Vol. 159, 1937.

5. PREISWERK, E. (1938). Application of the Methods of Gas Dynamics to Water Flows with a Free Surface. *Mitteilungen der Institut für Aerodynamik*, No. 7, E.T.H. Zürich, 1938. Translated as N.A.C.A. T.N. 934, 935, 1940.

6. —— (1939). Some Applications of the Method of Hydraulic Analogy. *Publications Scientifiques et Techniques du Ministère de l'Air*, pp. 43-77, No. 144, 1939.

7. —— (1942). *Brown-Boveri Revue*, Vol. 29, No. 1-3, p. 77, Jan.-March 1942.

8. ORLIN, W. J., LINDNER, N. J. and BITTERLY, J. G. (1947). Application of the Analogy between Water Flow with a Free Surface and Two-Dimensional Compressible Gas Flow. N.A.C.A. T.N. 1185, 1947, and also Report 875.

9. MATTHEWS, C. W. (1950). The Design, Operation and Uses of the Water Channel as an Instrument for the Investigation of Compressible Flow Phenomena. N.A.C.A. T.N. 2008, 1950.

10. TEOFILATO, S. (1949). A Contribution to the Study of Similarity between Hydro and Gas Dynamics. *Monografie Scientifiche di Aeronautica* (4) January, 1949.
TEOFILATO, P. (1949). *Monografie Scientifiche di Aeronautica* (5) 1947, (9) 1948, (10) 1949.

11. GILMORE, F. R., PLESSET, M. S. and CROSSLEY, H. E. (1950). The Analogy between Hydraulic Jumps in Liquids and Shock Waves in Gases. *Journal of Applied Physics*, pp. 243-249, Vol. 21, March 1950.

12. BERSHADER, D. (1949). Interferometric Study of Supersonic Channel Flow. *Review of Scientific Instruments*, p. 266, Vol. 20, April 1949.

13. HAVELOCK, T. H. (1908). Propagation of Groups of Waves in Dispersive Media. *Proc. Roy. Soc.* A. 81, pp. 398-430, 1908.

14. LAMB, H. (1932). *Hydrodynamics*. Cambridge University Press, 6th Ed., Chap. IX, 1932.

15. BAKHMETEFF, B. A. and MATZKE, A. (1935). The Hydraulic Jump in terms of Dynamic Similarity. *Transactions of the American Society of Civil Engineers*, pp. 630-680, Vol. 101, February 1935.

16. COURANT, R. and FRIEDRICHS, K. O. (1949). *Supersonic Flow and Shock Waves*. Interscience Publishers, 1st Ed., pp. 387-392, 1949.

17. FERRI, A. (1949). *Elements of Aerodynamics of Supersonic Flows*. Macmillan & Co., Chap. 8, 1949.

18. LIEPMANN, H. W. and BRYSON, A. E. (1950). Transonic Flow Past Wedge Sections. *Journal of the Aeronautical Sciences*, p. 750, Vol. 17, No. 12, December 1950.

19. BARDSLEY, O. and MAIR, W. A. (1951). The Interaction Between an Oblique Shock Wave and a Turbulent Boundary Layer. *Phil. Mag.*, Series 7, January 1951, Figure 10, p. 33.

CONTRACTING DUCTS OF FINITE LENGTH

by

L. G. WHITEHEAD, Ph.D.,

L. Y. WU, Ph.D.

and

M. H. L. WATERS, B.Sc.

(*Queen Mary College, London*)

SUMMARY

A method of design is given for wind tunnel contractions for two-dimensional flow and for flow with axial symmetry. The two-dimensional designs are based on a boundary chosen in the hodograph plane for which the flow is found by the method of images. The three-dimensional method uses the velocity potential and the stream function of the two-dimensional flow as independent variables and the equation for the three-dimensional stream function is solved approximately. The accuracy of the approximate method is checked by comparison with a solution obtained by Southwell's relaxation method.

In both the two and the three-dimensional designs the curved wall is of finite length with parallel sections upstream and downstream. The effects of the parallel parts of the channel on the rise of pressure near the wall at the start of the contraction and on the velocity distribution across the working section can therefore be estimated.

Typical designs are presented for contractions of moderate length which give small adverse pressure gradients on the walls and a uniform velocity distribution in the working section.

INTRODUCTION

The design of the contraction cone of a wind tunnel centres on the production of a steady stream with a uniform velocity distribution in the working section. The velocity distribution is associated directly with the shape of the contraction at its upstream end, while oscillations in the flow often arise from boundary layer separation near the start of the contraction caused by a too rapid change of section. In the present paper a method of design is given for contractions with circular cross-section and for two-dimensional flow at speeds for which compressibility effects are negligible. It enables good uniformity of velocity distribution at the exit to be achieved and boundary layer separation avoided in contractions of moderate length. Frictionless flow is assumed so that for a real fluid the shapes should be modified by a slight displacement of the wall outwards to allow for the boundary layer thickness.

Paper received March 1950.

[The Aeronautical Quarterly, Vol. II, February 1951]

The method has been applied initially to the design of a particular wind tunnel which has a contraction ratio of 7.25 and most of the examples in the paper relate to this design. Much larger contraction ratios, however, are well within its scope.

It might appear at first sight that little risk of boundary layer separation would arise in a contraction since a large pressure drop occurs as a result of the reduction of the cross-sectional area of the stream. In short contractions, however, as found by Batchelor and Shaw[1], a rise of pressure frequently occurs near the walls at the start of the contraction, followed by a rapid fall of pressure to a value lower than that of the final flow. Thus there are two regions of rising pressure where separation of the flow from the walls can occur, at the start and at the end of the contraction.

The two-dimensional flow problem is first considered and a series of contraction shapes giving a transition section of finite length from a parallel channel of given width to a narrower channel is developed from a simple boundary in the hodograph plane. Suitable choice of the parameters leads to contractions with small adverse pressure gradients and uniform velocity distribution in the working section. In the second part of the paper the flow with axial symmetry through these contraction shapes is calculated approximately. It is found that adverse pressure gradients are usually less than those for the two-dimensional flow and that favourable pressure gradients are increased. Boundary shapes which are satisfactory for two-dimensional channels therefore should have some extra margin of safety when used for tunnels of circular cross-section, in spite of the larger contraction ratio. The approximate solution depends on the close similarity which exists between the shapes of the streamlines for the two flows and becomes exact in certain simple cases. The accuracy of the approximation has been determined in a particular example by comparison with a numerically accurate solution obtained by Southwell's relaxation method.

Notation

a	length AB in the hodograph plane
b	length DE in the hodograph plane
	} *See* Fig. 3
h	resultant velocity of two-dimensional flow
k	two-dimensional contraction ratio (*see* Fig. 1)
q, q_1	complex variables in the hodograph plane
R	radius of the circular boundary in the hodograph plane
u, v	velocity components divided by U
U	velocity upstream of the contraction
V	resultant velocity of the three-dimensional flow
W	potential function for two-dimensional flow
$z=x+iy$	complex co-ordinates in the physical plane

α	velocity potential for two-dimensional flow
β	stream function for two-dimensional flow
γ, δ	constants defined in terms of a, b and R
μ, ν	constants defined in terms of γ, δ and $W=\alpha+i\beta$
ϕ	velocity potential for three-dimensional flow
ψ	Stokes' stream function for three-dimensional flow

SECTION I

TWO-DIMENSIONAL CONTRACTIONS

1.

The approximate solutions of the three-dimensional flow equation described in Section II require a knowledge of the two-dimensional velocity potential and stream function for the same boundary shapes. Existing methods are not entirely satisfactory for this purpose. Lighthill[2] gives a convenient method for determining the boundary shape for a chosen velocity distribution along the wall, but the calculation of the shape of the intermediate streamlines and the velocity distribution across the channel is difficult. The method given by Cheers[3] leads to contractions of too great an overall length and in addition only gives a curve approaching the parallel section at either end asymptotically. A third method suggested by Hughes[4], as giving the most rapid change of cross-section possible without reversal of pressure gradient, has a spiral discontinuity on the boundary so that it must be modified arbitrarily for practical applications. The present method avoids these defects.

2. *Flow in the hodograph plane*

The flow is first found in the hodograph plane where the co-ordinates are the velocity ratios u and $-v$. This choice is especially suitable in duct problems for the flow along a channel is represented in this plane by the flow from a source to a sink, and it is often possible to choose a simple boundary and determine the potential function by the method of images. Points at which the pressure gradient changes sign can also be found by inspection, since the radial distance from the origin represents the resultant velocity in the contraction cone.

The co-ordinates in the physical plane, shown in Fig. 1, are x and y. The channel has an initial width of $2k$, the velocity at this section is U and the two-dimensional contraction ratio is k. The channel wall in this z-plane and also in the hodograph plane is conveniently divided into four sections. The straight wall AB parallel to the axis, is followed by a curved section BC along which the vertical component of velocity increases to its maximum value at C. Along CD v decreases to zero and DE forms one side of the final parallel section. The corresponding configuration in the hodograph plane, defined by

$$q_1=u-iv=\frac{1}{U}\frac{dW}{dz}, \qquad . \quad . \quad . \quad . \quad (1)$$

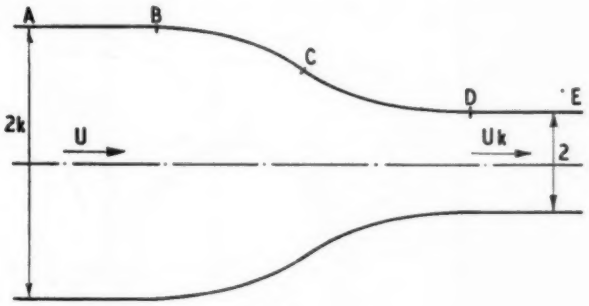

Fig. 1.
z-plane.

is shown in Fig. 2. W is the complex potential function in the z-plane and u and v are velocity ratios obtained by dividing the actual velocity components by U, the velocity at the beginning of the contraction. The upstream end of the contraction therefore corresponds to the point (1, 0) and the downstream end to the point (k, 0). The area between the curve BCD and the real axis transforms into the upper half of the contraction, AE corresponding to the centre line. The configuration chosen gives adverse pressure gradients along AB and DE but these appear to be unavoidable in a contraction with initial and final parallel sections. If adverse pressure gradients are to be entirely avoided, the boundary in the hodograph plane must lie on, or between, the two dotted circles of radii 1 and k centred at O, and this can only occur if A coincides with B and D with E. The boundary in the physical plane then becomes a continuous curve and the parallel sections are eliminated.

The shape of the boundary BCD must be selected to give a rapid contraction and this clearly requires as large a wall slope as possible near C. The simplest choice of a semi-circle for BCD is unsatisfactory as only a small vertical velocity component occurs at C. If, however, BCD is made a quadrant of a circle, as shown in Fig. 3, the maximum vertical velocity component is doubled and a contraction of sufficient rapidity results. The pressure along the curved wall then falls continuously from B to D.

The flow in the q_1-plane from the source at A to the sink at E can now be written down directly, six image sources and sinks being required to give the circular arc CD and the line BC as a streamline of the combined flow. The strengths of the sources and sinks are all equal and must be identical with the flow per unit time along the channel, *i.e.* $2Uk$. It is convenient now to shift the origin in the hodograph plane to B and to change the scale so that the circle is of unit radius. A new variable q is chosen therefore and is defined by the relation

$$q=(q_1-1+a)/R, \qquad (2)$$

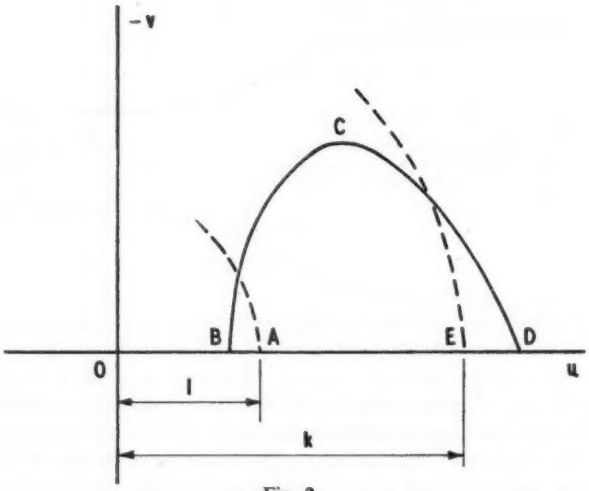

Fig. 2.
Hodograph plane.

where R, the radius of the circle in the q-plane, is given by

$$R=k+a+b-1,$$

and a and b are the lengths AB and DE, respectively. In terms of the new variable q the potential function then takes the form

$$\alpha+i\beta=W=\frac{Uk}{\pi}\log\frac{[q^2-a^2/R^2]\,[q^2-R^2/a^2]}{[q^2-\{(R-b)/R\}^2]\,[q^2-\{R/(R-b)\}^2]}. \qquad (3)$$

The velocity potential and the stream function for the two-dimensional flow are denoted here by α and β, respectively, to distinguish them from the corresponding functions ϕ and ψ for the axially symmetric flow. On the wall BC of the contraction, q is imaginary, so that β is zero; on the centre line q is real and lies in the range $a/R<q<(R-b)/R$, so that $\beta=-Uk$.

3. *Calculation of the boundary shape*

The flow in the z-plane is found by integrating the relation between dz/dq and q obtained by combining equations (1), (2) and (3). This can be done by re-arranging the equation and splitting into partial fractions but, since many terms result, the subsequent calculation of the shapes of individual streamlines is lengthy. Alternatively it is possible to make numerical integrations to determine the shape of any particular streamline directly from equation (3) and this procedure is usually more convenient.

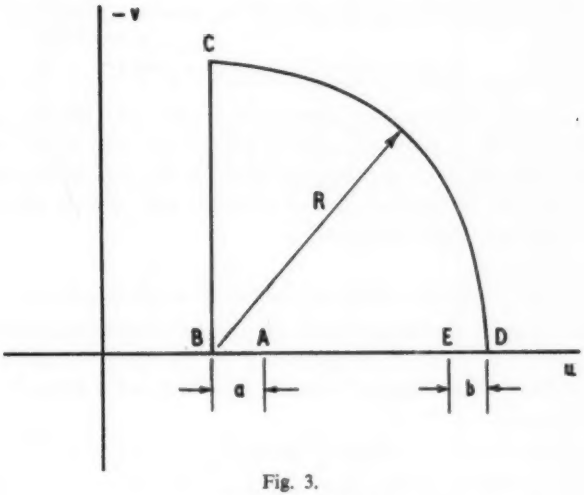

Fig. 3.
Hodograph plane.

The change in z along a streamline may be expressed directly in terms of the change in the velocity potential $\varkappa$ as

$$\delta z = \delta\varkappa/(dW/dz),$$

since β is constant. Substituting from (1) for dW/dz, separating into real and imaginary parts and integrating gives

$$x = \frac{1}{U}\int \frac{u}{u^2+v^2}\,d\varkappa\,, \quad y = \frac{1}{U}\int \frac{v}{u^2+v^2}\,d\varkappa. \qquad . \quad . \quad . \quad (4)$$

u and v are found from q for equal intervals of $\varkappa$ by re-arranging equation (3) in the form

$$q^4 - q^2\left(\frac{\gamma e^{\frac{\pi W}{Uk}} - \delta}{e^{\frac{\pi W}{Uk}} - 1}\right) + 1 = 0\,, \qquad . \quad . \quad . \quad . \quad . \quad (5)$$

where γ and δ are defined by

$$\gamma = \{(R-b)/R\}^2 + \{R/(R-b)\}^2\,, \quad \delta = (a/R)^2 + (R/a)^2\,.$$

The factor $\left(\gamma e^{\frac{\pi W}{Uk}} - \delta\right) \Big/ \left(e^{\frac{\pi W}{Uk}} - 1\right)$ is real on the outer wall and also on the centre line of the contraction, but complex for other streamlines. It is expressed generally

therefore as $2(\mu+i\nu)$, so that the solution of the quartic equation (5) becomes

$$q(2)^{\frac{1}{2}} = \pm(\mu+1+i\nu)^{\frac{1}{2}} \pm (\mu-1+i\nu)^{\frac{1}{2}}. \quad . \quad . \quad . \quad . \quad (6)$$

Equation (4) can now be integrated numerically. The only difficulty arises on the channel wall at C, where there is a rapid change in the slope of the wall. In this region smaller intervals of α are required than for the rest of the field and it is advantageous to start integrations from C as origin and proceed along the curved wall in both directions from this point.

4. *Simplified channels without parallel sections*

The elimination of the straight walls AB and DE simplifies the configuration in the q-plane considerably and the integration of the equations in complex form gives the shortest method of plotting the boundary. With a and b zero (3) becomes

$$W = \frac{2Uk}{\pi} \log \frac{q}{q^2-1}, \quad . \quad . \quad . \quad . \quad . \quad . \quad (7)$$

and hence

$$\frac{dW}{dq} = \frac{2Uk}{\pi}\left[\frac{1}{q} - \frac{1}{q-1} - \frac{1}{q+1}\right].$$

Also combining (1) and (2) gives for this simplified case

$$dW/dz = U[(k-1)\,q+1].$$

So that dz/dq takes the form

$$\frac{dz}{dq} = \frac{2k}{\pi}\frac{1}{(k-1)\,q+1}\left[\frac{1}{q} - \frac{1}{q-1} - \frac{1}{q+1}\right]. \quad . \quad . \quad . \quad . \quad (8)$$

This may be integrated directly giving

$$z = \frac{2}{\pi}\left[k\log q - \log(1-q) - \frac{k}{2-k}\log(1+q) + \frac{k^2-2k+2}{2-k}\log\{(k-1)\,q+1\}\right], \quad . \quad . \quad . \quad . \quad . \quad . \quad . \quad . \quad (9)$$

and it will be noted that the last two terms cancel in the special case $k=2$. The origin in the z-plane lies on the axis of symmetry because all the terms on the right hand side of equation (9) are real for q real and less than unity. The boundary of the contraction cone can now be plotted from (9) since q is known. For the intermediate streamlines equation (7) must be used in addition to determine values of q appropriate to the particular value of β required.

A typical contraction of this simplified type is shown in Fig. 4 together with the resultant velocity h along the wall and the centre line. The two-dimensional

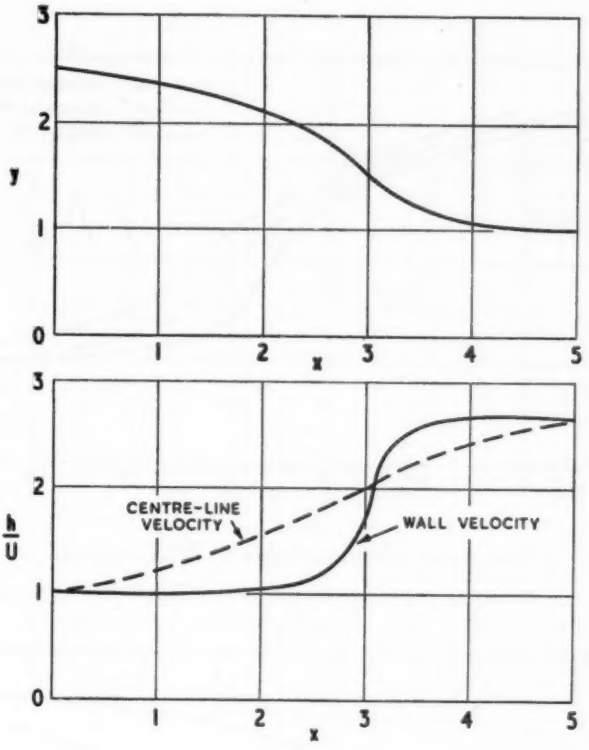

Fig. 4.
Long two-dimensional contraction without adverse pressure gradients.

contraction ratio in this example is 2.69, corresponding to the value 7.25 in a three-dimensional flow.

Figure 5 compares a duct having a contraction ratio of 4 with similar shapes given by Lighthill[2] and Cheers[3]. The present method is seen to give a more rapid change of cross-section near the centre of the range, but all three curves approach the limiting values slowly at the upstream and downstream ends. A further comparison of the three shapes is made in Fig. 6 which shows the maximum slope on the boundary for a range of contraction ratios.

5. *Examples with parallel walls upstream and downstream*

Examples giving a transition of finite length between parallel sections of differing width will now be considered. The length of the curved section *BD*, which

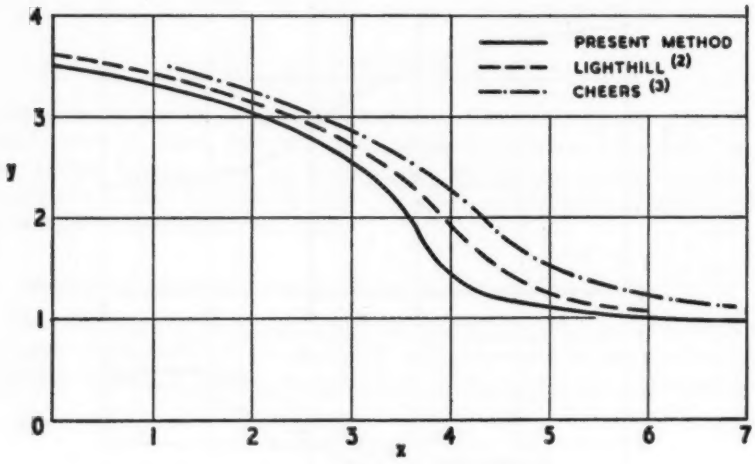

Fig. 5.

Comparison of contractions designed by different methods.

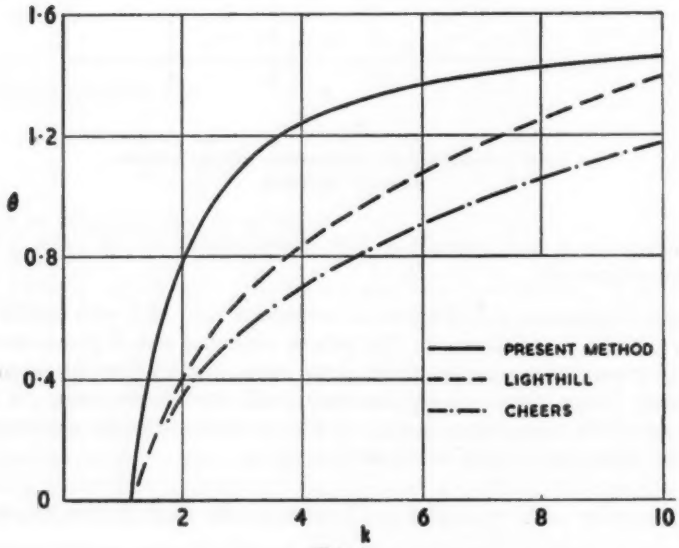

Fig. 6.

Comparison of maximum wall slope for different methods.

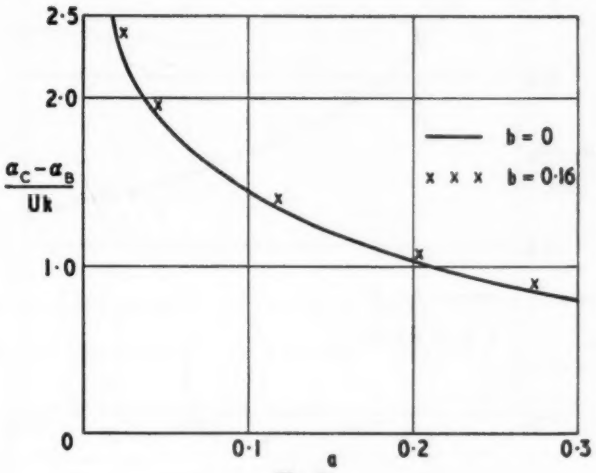

Fig. 7.
Influence of a on the length BC.

increases as a and b are reduced, is governed by the values chosen for the velocities at B and D. A rough measure of the length BC is given by the change in the velocity potential α between these points and this is given from (3) by the relationship

$$\alpha_C - \alpha_B = \frac{2Uk}{\pi} \log \frac{[R-b][R^2+a^2]}{a[(R-b)^2+R^2]}. \quad . \quad . \quad . \quad (10)$$

This change in α depends mainly on the value of a and is plotted, in Fig. 7, for a contraction ratio of 2.69. The small effect of varying b is shown by the difference between the full line for $b=0$ and the crosses corresponding to $b=0.16$.

The corresponding relation for $\alpha_D - \alpha_C$

$$\alpha_D - \alpha_C = \frac{2Uk}{\pi} \log \frac{[R^2-a^2][R^2+(R-b)^2]}{[R^2+a^2][R^2-(R-b)^2]} \quad . \quad . \quad . \quad (11)$$

is plotted in Fig. 8 and the main variable in this case is b. Values for higher contraction ratios can be found from these curves by increasing a and b in proportion to $k-1$.

The choice of a suitable value for a must be settled as a compromise between the length of the curved wall and the adverse pressure gradient near B caused by the velocity falling to $U(1-a)$. A typical contraction is shown in Fig. 9, in which the curved wall BD is plotted. The value of k is 2.69 and the total change of the velocity potential between B and D has been taken at $4Uk$. For this example a is equal to b and their value is 0.055, so that a rise of pressure of about 11 per cent. of the total head occurs on the straight wall near B.

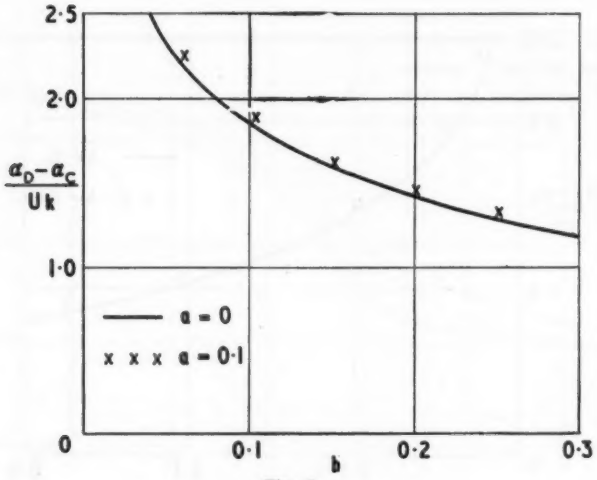

Fig. 8.
Influence of b on length $C\,D$.

The value of b, in addition to varying the adverse pressure gradient beyond D, influences the rapidity with which a uniform flow is produced in the high speed section of the duct. In order to examine this effect, a further example has been considered which is similar to that shown in Fig. 9 except that b has been trebled. The change in α is reduced to $3.35Uk$ and the overall length of the contraction is reduced to 5.75, on the scale used in Fig. 9, due to a shortening of the curved wall CD. The difference between the centre line velocity at the start of the parallel section and the final value Uk amounts to 2.5 per cent. compared with one per cent. for the longer contraction. When the velocity distributions are compared on the basis of equal distances from the start of the contraction, however, the shorter contraction with the larger value of b is found to be superior. For values of $x>6$ the centre-line velocity differs from its final value by less than half the amount that it does for corresponding points on the curve shown in Fig. 9. It appears therefore that a gradual approach to the final parallel section is not advantageous, since it delays the rise in the centre-line velocity. A considerable increase of b is not permissible however, as the larger adverse pressure gradient on the wall would be likely to cause separation.

SECTION II

THREE-DIMENSIONAL FLOW

1.

The approximate method described in this section enables the three-dimensional flow to be calculated through contraction cones, of circular cross-section, identical in shape with the two-dimensional boundaries in Section I. The velocity potential α and the stream function β of the two-dimensional flow are used as co-ordinates and

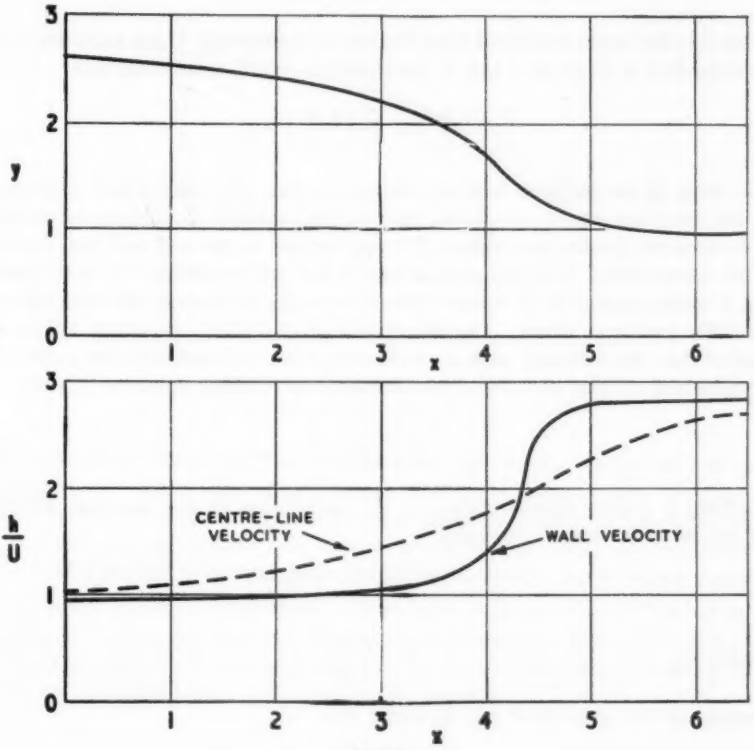

Fig. 9.
Two-dimensional contraction of finite length.

the method is basically similar to that employed by Fox and Southwell[5] for the calculation of the transonic flow through a convergent-divergent nozzle.

With earlier methods such as those of Tsien[6] and Szczeniowski[7] it is not possible to investigate the effects of the parallel section upstream and downstream of the contraction. Thwaites'[8] method, in which contractions and expansions are repeated cyclically, appears to over-estimate the drop in velocity on the wall at the start of the contraction and to under-estimate the rapidity with which the velocity approaches uniformity at the high speed end. Contraction cones designed on this basis therefore will be unnecessarily long.

2. *Equations for the stream function*

The equation for Stokes' stream function ψ for axially symmetric flow takes the form

$$\frac{\partial}{\partial x}\left(\frac{1}{y}\frac{\partial \psi}{\partial x}\right)+\frac{\partial}{\partial y}\left(\frac{1}{y}\frac{\partial \psi}{\partial y}\right)=0, \quad . \quad . \quad . \quad . \quad (12)$$

where y is the height measured from the axis of symmetry. If the variables x and y are expressed in terms of α and β, the equation readily transforms into

$$\frac{\partial}{\partial\alpha}\left(\frac{1}{y}\frac{\partial\psi}{\partial\alpha}\right)+\frac{\partial}{\partial\beta}\left(\frac{1}{y}\frac{\partial\psi}{\partial\beta}\right)=0. \quad . \quad . \quad . \quad . \quad . \quad (13)$$

This form of the equation is more convenient than (12) when α and β are known for the boundary shape considered, because the boundary conditions are simplified to $\psi=$constant for the two values of β appropriate to the wall and the centre line of the contraction. The wall and the centre line are streamlines for both flows, so that it seems reasonable to assume that the two sets of intermediate streamlines will not differ greatly in shape. The rate of change of ψ with α therefore will be much smaller than the variation with β. Following Fox and Southwell the α derivatives are neglected entirely as a first approximation, so reducing equation (13) to

$$\frac{\partial}{\partial\beta}\left(\frac{1}{y}\frac{\partial\psi}{\partial\beta}\right)=0. \quad . \quad . \quad . \quad . \quad . \quad (14)$$

Applying a similar approximation in the calculation of the resultant velocity V for the flow, the exact expression

$$V^2=\frac{h^2}{y^2}\left[\left(\frac{\partial\psi}{\partial\alpha}\right)^2+\left(\frac{\partial\psi}{\partial\beta}\right)^2\right],$$

reduces to

$$V=\frac{h}{y}\frac{\partial\psi}{\partial\beta}. \quad . \quad . \quad . \quad . \quad . \quad . \quad (15)$$

Comparing (14) and (15) it will be noted that

$$\frac{\partial}{\partial\beta}\left(\frac{V}{h}\right)=0,$$

hence to this order of approximation, V/h, the ratio of the resultant velocities for the two-dimensional and the three-dimensional flows, is a function of α only. Therefore

$$\frac{V}{h}=f(\alpha)=\frac{1}{y}\frac{\partial\psi}{\partial\beta}, \quad . \quad . \quad . \quad . \quad . \quad (16)$$

and integrating along an $\alpha=$constant line leads to

$$\psi=f(\alpha)\int y\,d\beta.$$

If ψ is chosen as zero along the centre line, its value on the outer wall will be $Uk^2/2$ so that integrating across the channel yields the value of $f(\alpha)$ in the form

$$\frac{Uk^2}{2}=f(\alpha)\int_{-Uk}^{0} y\,d\beta. \quad . \quad . \quad . \quad . \quad . \quad (17)$$

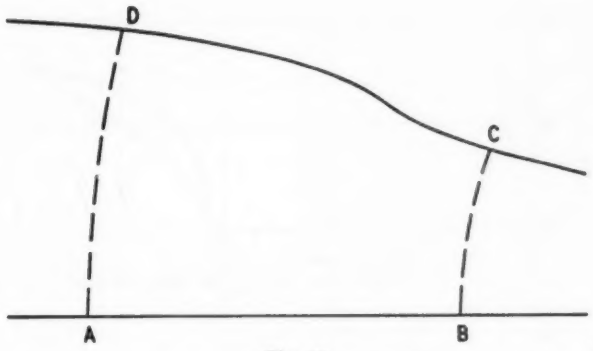

Fig. 10.
Contour for evaluation of $f(\alpha)$.

Closer approximations to the flow may be found by substituting for the first term in equation (13) values appropriate to the first approximation and solving this modified form. This procedure has not been adopted because it has been found, by comparing a representative case with a numerically accurate solution obtained by Southwell's relaxation method, that the first approximation has adequate accuracy.

The direct numerical evaluation of the velocity ratio $f(\alpha)$ from (17) involves the calculation of values of y at a number of points along each α line. It is often more convenient to express the integral $\int y\,d\beta$ in terms of the values of $\int x\,d\alpha$ taken along the wall and the centre line. Consider first the integral

$$\int (x+iy)(d\alpha+id\beta),$$

taken around the contour $ABCD$ shown in Fig. 10, AB lying along the centre line of the contraction and CD along the wall. Since there are no singularities in the integrand within the area considered the integral is zero, so that its real part is zero. Thus

$$\int (xd\alpha+yd\beta)=0\ ,$$

and hence, since β is constant along AB and CD and α is constant along BC and AD,

$$\int_B^C yd\beta=\int_A^D yd\beta-\int_A^B xd\alpha+\int_D^C xd\alpha\,.$$

Only one integration across the stream therefore is required and this is conveniently made along the line $\alpha=0$. The further integrations with respect to α make use ot data already found in determining the boundary shape and velocity distribution from the hodograph plane.

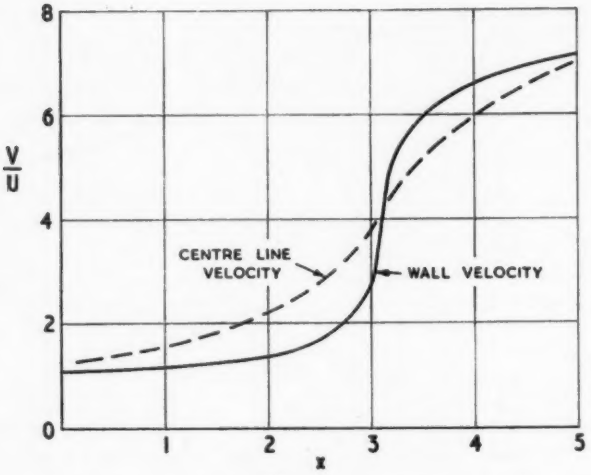

Fig. 11.
Three-dimensional velocity distribution for long contraction.

3. *Examples of three-dimensional contractions*

Examples of three-dimensional velocity distributions calculated in this way are shown in Figs. 11 and 12. Fig. 11 shows the wall and centre-line velocities for the simple contraction without parallel sections illustrated in Fig. 4, and Fig. 12 gives the three-dimensional velocity distribution for the finite contraction shown in Fig. 9. In each case the contraction ratio now becomes $k^2=7.25$. For the first example there is no adverse pressure gradient in the two-dimensional flow and none arises in the three-dimensional case; in fact moderate favourable pressure gradients replace the small favourable pressure gradients existing in the two-dimensional flow at each end of the figure. For the second example the adverse pressure gradients for the axi-symmetric flow are no greater than for the two-dimensional flow and the favourable pressure gradients are increased.

4. *Exact solutions*

It is of interest to note that the approximate solution of (13) becomes exact in special cases for which y may be expressed as a product of a function of α multiplied by a function of β. A simple channel of this type is the converging-diverging hyperbolic nozzle for which

$$y=\cosh \alpha \sin \beta .$$

Other exact solutions of flow with axial symmetry depending on the existence of a simple relation between y, α and β are given by Milne-Thomson[9].

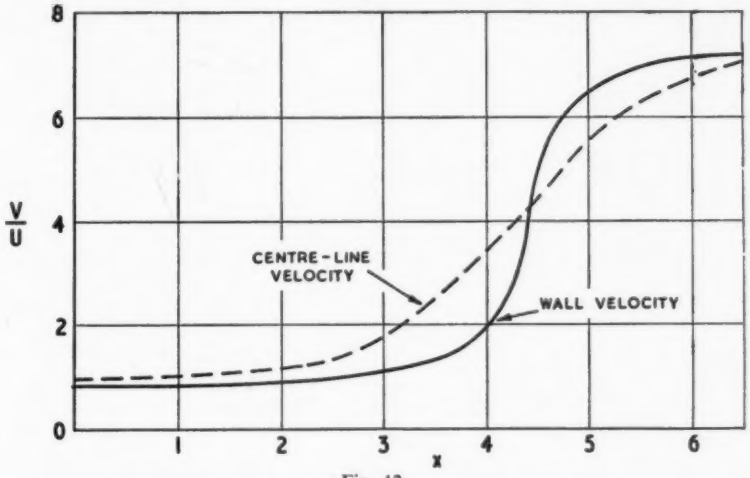

Fig. 12.

Three-dimensional velocity distribution for finite contraction.

5. *Numerical solution by relaxation method*

The relaxation method has been employed to provide a numerical check on the results shown in Fig. 11. The equations (12) and (13) are of the quasi-plane harmonic type considered by Southwell[10] so that the method need not be described here in detail. Relaxation methods have previously been employed in the calculation of the flow in a wind tunnel contraction by Batchelor and Shaw who solved equation (12) for a particular boundary. In the present case equation (13) has been employed on account of the much simpler boundary conditions. The area over which the relaxation solution has to be determined in the α, β plane is a rectangle and all irregular stars are avoided. Equation (13) may be arranged in the form

$$\nabla^2 y\psi - 3y\nabla^2\psi - \psi\nabla^2 y = 0,$$

where ∇^2 denotes $\dfrac{\partial^2}{\partial\alpha^2} + \dfrac{\partial^2}{\partial\beta^2}$. The residual F, at a point in a square mesh, is therefore given by

$$F = \sum_1^4 (y\psi) - 3y_0 \sum_1^4 \psi - \psi_0 \sum_1^4 y + 12\,\psi_0 y_0,$$

where the suffix 0 denotes the centre point of the star and the suffixes 1 to 4 the outer points. The corresponding relaxation pattern is shown in Fig. 13. Intervals of α and β of $Uk/6$ were chosen and the approximate solution was used to give the

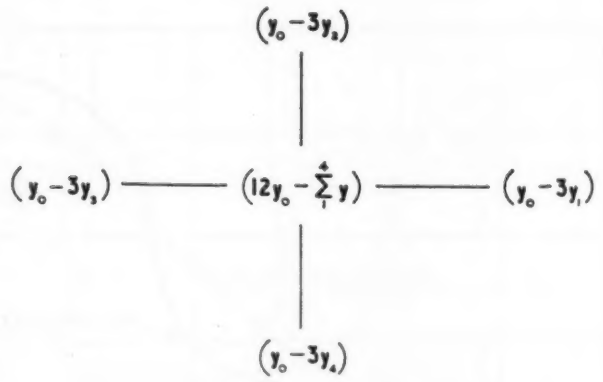

Fig. 13.
Relaxation pattern for unit change of ψ.

initial values of ψ. The small residuals were then quickly liquidated. The approximate and accurate values of ψ are compared in Table I for the particular α line passing through C where the wall slope is a maximum and where the largest residuals occur. Very close agreement is shown, so that the estimated velocity distribution can be used with confidence.

TABLE I

β/Uk	-1	$-\frac{5}{6}$	$-\frac{2}{3}$	$-\frac{1}{2}$	$-\frac{1}{3}$	$-\frac{1}{6}$	0
Approximate value $\frac{2{,}000\psi}{Uk^2}$	0	29	114	256	453	703	1,000
Accurate value $\frac{2{,}000\psi}{Uk^2}$	0	28.7	114.3	256.1	452.6	702.3	1,000

CONCLUSIONS

A method of two-dimensional design for wind tunnel contractions has been developed which gives a rapid change of cross-section with small adverse pressure gradients. The contractions are of finite length and the channel has parallel walls upstream and downstream of the curved section. An approximate method of satisfactory accuracy is given for finding the flow with axial symmetry through channels designed by the two-dimensional method. Boundary shapes satisfactory in two dimensions are also satisfactory for three-dimensional channels with axial symmetry. Estimation of the adverse pressure gradient at the start of the contractions and the uniformity of velocity distribution across the working section

require a method in which the parallel sections of the tunnel are represented. A too gradual transition to the parallel working section delays the development of a uniform velocity distribution across the working section and increases the length of the contraction unnecessarily. The use of a three-dimensional method which takes account of results found for two-dimensional flow leads to the design of satisfactory contractions of short overall length.

REFERENCES

1. BATCHELOR, G. K. and SHAW, F. S. (1944). A Consideration in the Design of Wind Tunnel Contractions. Australian Report A.C.A.4, 1944.
2. LIGHTHILL, M. J. (1945). A New Method of Two-dimensional Aerodynamic Design. R. & M. 2112, 1945.
3. CHEERS, F. (1945). Note on Wind Tunnel Contractions. R. & M. 2137, 1945.
4. HUGHES, N. J. S. (1944). Stream Expansion with a Discontinuity in Velocity on the Boundary. R. & M. 1978, 1944.
5. FOX, L. and SOUTHWELL, R. V. (1944). On the Flow of a Gas through a Nozzle with Velocities Exceeding the Speed of Sound. *Proc. Roy. Soc.* A.183, pp. 38-54, 1944.
6. TSIEN, H. S. (1943). On the Design of a Contraction Cone for a Wind Tunnel. *Journal of the Aeronautical Sciences*, Vol. 10, pp. 68-70, 1943.
7. SZCZENIOWSKI, B. (1943). Contraction Cone for a Wind Tunnel. *Journal of the Aeronautical Sciences*, Vol. 10, pp. 311-313, 1943.
8. THWAITES, B. (1946). On the Design of Wind Tunnel Contractions. R. & M. 2278, 1946.
9. MILNE-THOMPSON, L. (1950). *Theoretical Hydrodynamics* (2nd edition) (Chap. XV). Macmillan & Co., 1950.
10. SOUTHWELL, R. V. (1946). *Relaxation Methods in Theoretical Physics* (Chap. 5). Clarendon Press, 1946.

THE PROPERTIES OF CROSSED FLEXURE PIVOTS, AND THE INFLUENCE OF THE POINT AT WHICH THE STRIPS CROSS

by

W. H. WITTRICK, M.A., A.F.R.Ae.S.
(Senior Lecturer, Department of Aeronautics, University of Sydney)

SUMMARY

It is shown that the rotational stiffness of a crossed flexure pivot varies considerably when subjected to an applied force. The type of variation can be radically changed simply by moving the point at which the strips cross. The relation between torque and rotation for a given applied force is not exactly linear and the extent of the non-linearity is determined by taking into account the small movements of the centre of rotation of the pivot. Finally, for design purposes, an analysis of the maximum stresses in the strips is given.

1. INTRODUCTION

Crossed flexure pivots, of the type shown in Fig. 1, are extensively used in aeronautical research equipment to replace knife edges or ball bearings. Perhaps the most frequent use is for the fulcrum of the balance arm in a wind tunnel balance. Here, a null-point method of reading is almost invariably used, so that the prime considerations influencing the design of a flexure pivot for such a purpose are (*a*) that the applied loads should not cause instability of the pivot, and (*b*) that the rotational stiffness should be small enough to give adequate sensitivity. If changes in the applied load (*e.g.* the lift) should cause changes in the tension or compression in the strips of sufficient magnitude to give a noticeable change in rotational stiffness, the only effect would be a change in the sensitivity of the balance, with little or no change in the overall accuracy of the reading.

There are many cases where changes in rotational stiffness affect directly the accuracy of the experimental readings. The present investigation, for example, arose primarily out of an experimental determination of the stability derivative l_p. The technique employed consisted of forcing the model to perform rolling oscillations about its longitudinal axis, and the model had therefore to be mounted in such a way that these oscillations could take place. The obvious way to

Paper received February 1950.

[The Aeronautical Quarterly, Vol. II, February 1951]

implement this was by means of ball bearings. It was found, however, that the dust in the tunnel air made the ball bearings by no means frictionless, and in an attempt to overcome this they were replaced by flexure pivots, in which the strips were perpendicular to each other and crossed at their middle points. It was then found that the wide variations in the aerodynamic forces on the model gave large changes in the rotational stiffness of the pivots and their use was finally abandoned in favour of ball bearings.

The behaviour of such symmetrical flexure pivots, in which the strips cross at their middle points, under a combination of vertical and horizontal loads, was discussed by the author in a previous paper[1]. It was assumed throughout that the rotation θ was small enough to be neglected in comparison with unity. With this approximation it was shown that the centre of rotation of the moving end of the pivot remained fixed at the point at which the undeflected strips crossed and, further, that the ratio between the shear force and tension in a strip was equal to $\theta/2$. The shear forces were neglected therefore and the tensions could then be obtained in terms of the applied load. These tensions were independent of the angle of rotation and the resulting relation between the rotation and the applied torque (about the centre of rotation) was linear. The analysis, confirmed by experiment, showed that considerable variations of rotational stiffness with applied force occur, and the pivot can become unstable, that is have a negative restoring torque, with the strips either in tension or compression.

A recent paper by Haringx[2] discusses this identical problem, and derives results exactly similar to those mentioned above. He also considers the case of large rotations when the pivot is subjected to a pure torque only, with no applied forces. His results show that the ratio between the torque and rotation is not constant, but increases as the rotation increases. With the strips crossing at right angles the linear theory, assuming small deflections, underestimates the restoring torque by about 10 per cent. when the rotation is 45°.

The present paper is concerned primarily with an investigation of the effect of changing the point at which the strips cross. It is shown that by adopting this simple expedient the variation of rotational stiffness with applied force can be altered radically. For example, by crossing the strips at one end, the pivot never becomes unstable with the strips in tension, although large variations of stiffness with applied force still occur. There is one pivot, however, in which the strips cross at 87.3 per cent. $(=1/2+\sqrt{5}/6)$ of the distance along each strip, which appears to be superior in all respects. If the applied forces are not too great the centre of rotation remains fixed to a much higher order of accuracy than in other pivots. As a direct result of this the rotational stiffness remains sensibly constant over an appreciable range of vertical force.

As a secondary consideration the linearity of the torque-rotation curve is investigated. It is shown that the departures from linearity are greater with, than without, a side force acting on the pivot.

The paper concludes with an analysis of the maximum stresses in the strips, for design purposes.

Notation

L	length of each flexure strip
b	total width of flexure strips on each side of the pivot
t	thickness of each flexure strip
α	inclination of each strip to the vertical
ρ	a parameter whose value defines the point at which the undeflected strips cross (Fig. 1)
I	$bt^3/12$. Relevant moment of inertia of the cross section of the strips on each side of the pivot
E	Young's modulus of the material
θ	rotation of the moving end of the pivot
δ	lateral deflection of the moving end of a strip
ξ	$2\delta/(\theta L)-1-\rho$
e	shortening of a strip due to change of slope
λ	$e/(\theta^2 L)$. Given by equation (24)
y	lateral deflection of a strip at a distance x from its fixed end
X	x/L
P	tension in a strip
F	shear force in a strip
β	$[PL^2/(4EI)]^{\frac{1}{2}}$
γ	$[-PL^2/(4EI)]^{\frac{1}{2}}$
γ_s	value of γ at which m_s first occurs
f	$FL^2/(EI)$
M	bending moment in a strip at a distance x from its fixed end
M_o	moment of the terminal forces in a strip about the point at which the undeflected strips cross
m	$ML/(EI)$
m_s	stationary value of m. *See* Section 6
V	vertical component of the forces applied to the moving end of the pivot, positive when inducing tension in the strips
H	horizontal component of the forces applied to the moving end of the pivot

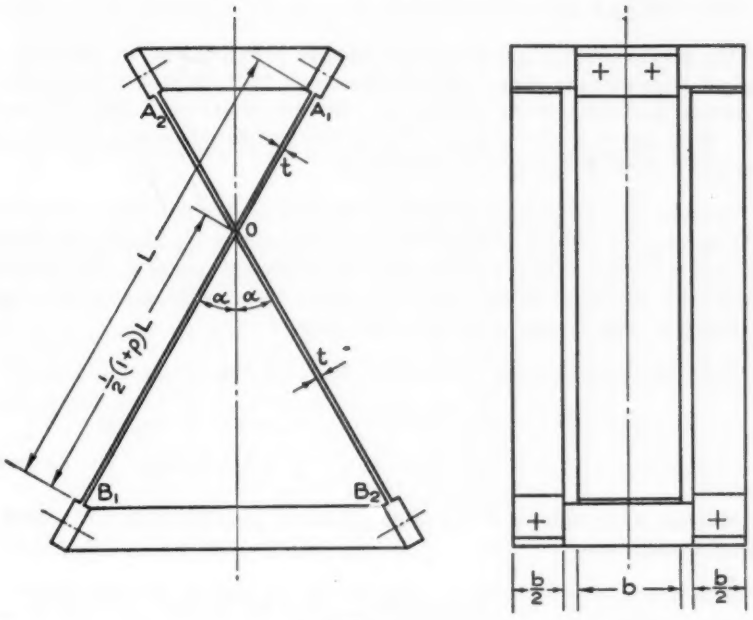

Fig. 1.
Typical crossed flexure pivot.

v $VL^2 \sec \alpha/(EI)$

h $HL^2 \operatorname{cosec} \alpha/(EI)$

T applied torque about the point at which the undeflected strips cross

ψ $\beta^2+\rho\beta^3/(\beta-\tanh\beta)$

ϕ $\beta(\coth\beta-\beta)+\rho^2\beta^3/(\beta-\tanh\beta)$

K, b coefficients in the relation between torque and rotation. *See* equation (27)

K_0 value of K when $V=H=0$

Suffixes A, B refer to the fixed and moving ends of a strip respectively.

Suffixes 1, 2 refer to the strips on the two sides of the pivot. Strip No. 1 is that in which the horizontal force H is inducing tension.

Suffix O refers to the point O at which the undeflected strips cross.

2. THE CENTRE OF ROTATION

The pivot under consideration is of the type shown in Fig. 1. The strips are arranged symmetrically about both vertical centre lines, inclined at an angle α to the vertical and cross at the point O at a distance of $\frac{1}{2}(1+\rho)L$ from the moving ends. Note that if $\rho=0$ the strips cross at their middle points and if $\rho=\pm 1$ they cross at the fixed or moving ends respectively.

Consider now the pivot in a displaced position as shown in Fig. 2, the rotation of the moving end being θ. The points B_1 and B_2 move to B_1' and B_2', the tangents $B_1'G$ and $B_2'G$ then making angles θ with the undeflected positions. The transverse deflections δ_1 and δ_2 are of the order of θL whilst the shortenings e_1 and e_2, due to the change of slope of each strip, are of the order of $\theta^2 L$.

If the moving end is rigid, then $B_1B_2=B_1'B_2'$, giving

$$(1+\rho)^2 L^2 \sin^2\alpha = \{(1+\rho)L\sin\alpha-(\delta_1-\delta_2)\cos\alpha-(e_1+e_2)\sin\alpha\}^2 + \{(\delta_1+\delta_2)\sin\alpha-(e_1-e_2)\cos\alpha\}^2.$$

If terms of the order of θ^3 are neglected on the assumption that θ is small this expression reduces to

$$2(1+\rho)L\{(\delta_1-\delta_2)+(e_1+e_2)\tan\alpha\} = (\delta_1+\delta_2)^2\tan\alpha+(\delta_1-\delta_2)^2\cot\alpha. \qquad (1)$$

Also, since the rotation of the moving end is θ,

$$(\delta_1+\delta_2)\sin\alpha-(e_1-e_2)\cos\alpha=(1+\rho)L\sin\alpha\sin\theta.$$

Neglecting terms of order θ^3 we have $\sin\theta=\theta$, and the last equation gives

$$(\delta_1+\delta_2)-(e_1-e_2)\cot\alpha=(1+\rho)\theta L. \qquad (2)$$

Squaring both sides of equation (1), it is seen that

$$(\delta_1-\delta_2)^2=O(\theta^4), \qquad (3)$$

and similarly from equation (2)

$$(\delta_1+\delta_2)^2=(1+\rho)^2\theta^2L^2+O(\theta^3). \qquad (4)$$

Substituting (3) and (4) into the right hand side of (1) and neglecting terms of order θ^3 we obtain

$$(\delta_1-\delta_2)+(e_1+e_2)\tan\alpha=\tfrac{1}{2}(1+\rho)\theta^2L\tan\alpha. \qquad (5)$$

Writing $e=\lambda\theta^2 L$, equations (2) and (5) when solved for δ_1 and δ_2 give

$$\left.\begin{aligned}\delta_1&=\tfrac{1}{2}(1+\rho)\theta L+\{\tfrac{1}{4}(1+\rho)\tan\alpha+\lambda_1\cot 2\alpha-\lambda_2\operatorname{cosec}2\alpha\}\theta^2 L\\ \delta_2&=\tfrac{1}{2}(1+\rho)\theta L-\{\tfrac{1}{4}(1+\rho)\tan\alpha+\lambda_2\cot 2\alpha-\lambda_1\operatorname{cosec}2\alpha\}\theta^2 L\end{aligned}\right\} \quad . \qquad (6)$$

It will be seen from equations (6) that if the terms in θ^2 are neglected, then

$$\delta_1=\delta_2=\tfrac{1}{2}(1+\rho)\theta L,$$

indicating that the point G coincides with O. Consequently, to the first order, the centre of rotation of the pivot is fixed. However, in order to deal with the non-linearity of the relation between torque and rotation it is necessary to retain the terms in θ^2, thereby taking into account the movement of the centre of rotation.

It should be noted that in the particular case of a pivot in which the strips cross at right angles ($\alpha=45°$), equations (6) simplify to

$$\left.\begin{aligned}\delta_1&=\tfrac{1}{2}(1+\rho)\theta L+\{\tfrac{1}{4}(1+\rho)-\lambda_2\}\theta^2 L\\ \delta_2&=\tfrac{1}{2}(1+\rho)\theta L-\{\tfrac{1}{4}(1+\rho)-\lambda_1\}\theta^2 L\end{aligned}\right\} \quad . \quad . \quad . \qquad (7)$$

3. THE FORCES IN THE STRIPS

Suppose that the moving end of the pivot is subjected to a system of forces whose resultant has vertical and horizontal components V and H through the point O, together with a torque T about this point, as shown in Fig. 3. The force V is positive when it is tending to induce tension in the strips but negative values must also be considered. The force H can be limited to positive values only, since the pivot is symmetrical about the vertical centre line and its behaviour as a whole is therefore independent of the direction of H.

If P_1, P_2 and F_1, F_2 are the tensions and shear forces (referred to the undeflected directions) in the two strips, we have for equilibrium

$$\left.\begin{aligned}V&=(P_1+P_2)\cos\alpha+(F_1-F_2)\sin\alpha\\ H&=(P_1-P_2)\sin\alpha-(F_1+F_2)\cos\alpha\end{aligned}\right\} \quad . \quad . \quad . \quad . \qquad (8)$$

It is convenient to express these equations non-dimensionally by writing

$$\left.\begin{aligned}v&=\frac{VL^2}{EI}\sec\alpha, & h&=\frac{HL^2}{EI}\operatorname{cosec}\alpha\\ 4\beta^2&=\frac{PL^2}{EI}, & f&=\frac{FL^2}{EI}\end{aligned}\right\} \quad . \quad . \quad . \qquad (9)$$

where EI $(=Ebt^3/12)$ is the total flexural rigidity of the strips on each side of the pivot.

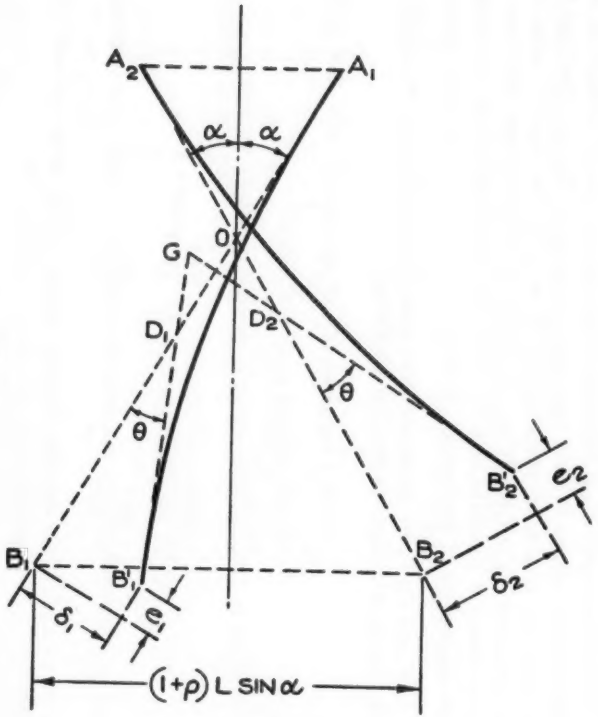

Fig. 2.
The displaced pivot.

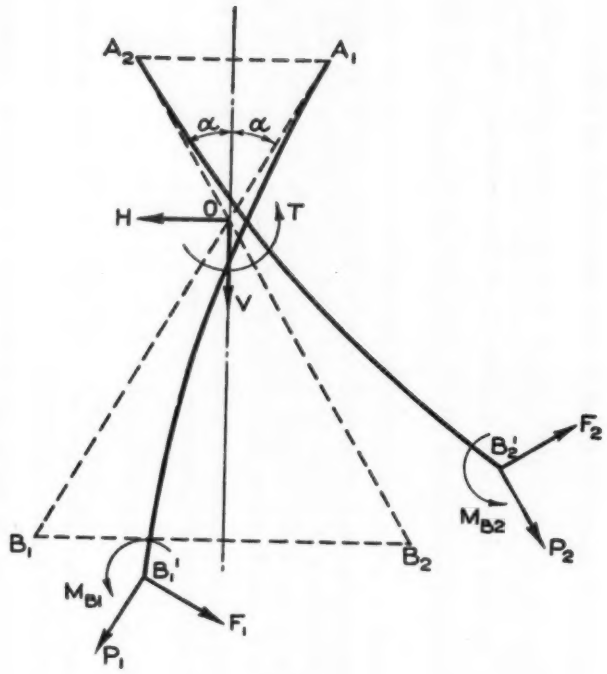

Fig. 3.
Forces and moments on displaced pivot.

Equations (8) then become

$$4(\beta_1^2+\beta_2^2)=v-(f_1-f_2)\tan\alpha,$$
$$4(\beta_1^2-\beta_2^2)=h+(f_1+f_2)\cot\alpha.$$

On solving for β_1^2 and β_2^2 we obtain

$$\left.\begin{aligned}4\beta_1^2&=\tfrac{1}{2}(v+h)+f_1\cot 2\alpha+f_2\operatorname{cosec}2\alpha\\ 4\beta_2^2&=\tfrac{1}{2}(v-h)-f_1\operatorname{cosec}2\alpha-f_2\cot 2\alpha\end{aligned}\right\} \quad . \quad . \quad . \quad (10)$$

In order to determine β_1 and β_2 completely, more information about the magnitudes of the shear forces is required.

Let M_{O1} and M_{O2} be the moments about the point O of the forces in the strips at B_1' and B_2' respectively so that

$$\begin{aligned}M_{O1}&=M_{B1}+\tfrac{1}{2}(1+\rho)F_1L-P_1\delta_1\\&=M_{A1}-\tfrac{1}{2}(1-\rho)F_1L,\end{aligned}$$

with similar expressions for M_{O2}. Then the torque T is given simply by the equation

$$T=M_{O1}+M_{O2}. \quad . \quad . \quad . \quad . \quad . \quad . \quad (11)$$

To proceed further it is now necessary to consider the bending of a single strip in detail, as shown in Fig. 4. The differential equation to be satisfied by the deflection y at a distance x from the fixed end A is

$$EI\frac{d^2y}{dx^2}=Py+M_A-Fx.$$

On multiplying throughout by $L^2/(EI)$ and writing $X=x/L$, $m_A=M_AL/(EI)$ we obtain the equation

$$\frac{d^2y}{dX^2}-4\beta^2y=L(m_A-fX),$$

where β and f are given by equations (9).

The general solution of this equation is

$$y=Q\sinh 2\beta X+R\cosh 2\beta X+\frac{L}{4\beta^2}(fX-m_A). \quad . \quad . \quad . \quad (12)$$

The conditions of zero deflection and slope at the end A ($X=0$) give

$$Q=\frac{-fL}{8\beta^3}, \qquad R=\frac{m_AL}{4\beta^2} \quad . \quad . \quad . \quad . \quad (13)$$

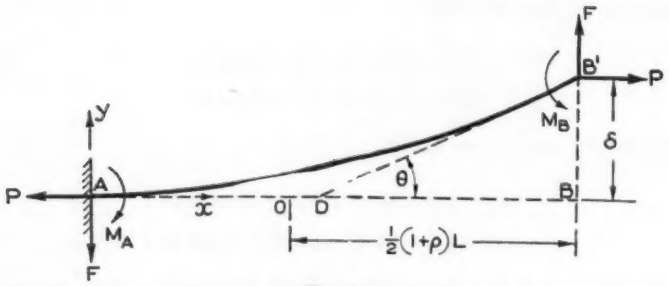

Fig. 4.
The bending of a single strip.

Also, at the end $B(X=1)$ we have $y=\delta$ and $dy/dx=\theta$, giving the two equations

$$\frac{\delta}{L}=\frac{m_A}{4\beta^2}(\cosh 2\beta-1)-\frac{f}{8\beta^3}(\sinh 2\beta-2\beta)$$

$$\theta=\frac{m_A}{2\beta}\sinh 2\beta-\frac{f}{4\beta^2}(\cosh 2\beta-1).$$

On solving for m_A and f we obtain

$$m_A=\theta\left\{\beta\coth\beta+(\rho+\xi)\frac{\beta^2\tanh\beta}{\beta-\tanh\beta}\right\} \quad . \quad . \quad . \quad (14)$$

$$f=\theta\left\{2\psi+2\xi\frac{\beta^3}{\beta-\tanh\beta}\right\}, \quad . \quad . \quad . \quad . \quad (15)$$

where
$$\psi=\beta^2+\frac{\rho\beta^3}{\beta-\tanh\beta} \quad . \quad . \quad . \quad . \quad . \quad (16)$$

and
$$\xi=\frac{2\delta}{\theta L}-1-\rho. \quad . \quad . \quad . \quad . \quad . \quad (17)$$

It will be seen from equations (6) that ξ is of the order of θ.

The bending moment M at any point in the strip is given non-dimensionally by

$$m=\frac{ML}{EI}=\frac{1}{L}\frac{d^2y}{dX^2}.$$

By virtue of equations (12) and (13) this becomes

$$m=m_A\cosh 2\beta X-\frac{f}{2\beta}\sinh 2\beta X. \quad . \quad . \quad . \quad . \quad (18)$$

On using equations (14) and (15) this may be put in the form

$$m=\theta\left\{\beta\,\mathrm{cosech}\,\beta\cosh\beta(1-2X)+(\rho+\xi)\frac{\beta^2\,\mathrm{sech}\,\beta}{\beta-\tanh\beta}\sinh\beta(1-2X)\right\}. \quad (19)$$

The bending moment M_B at the end B, obtained by putting $X=1$ in equation (19), is given non-dimensionally by

$$m_B=\theta\left\{\beta\coth\beta-(\rho+\xi)\frac{\beta^2\tanh\beta}{\beta-\tanh\beta}\right\}. \quad . \quad . \quad . \quad (20)$$

Also the moment M_O of the terminal forces about the point O at which the undeflected strips cross, is given by

$$m_O=M_OL/(EI)=m_A-\tfrac{1}{2}(1-\rho)f.$$

Using (14) and (15) this becomes

$$m_O=\theta\{\phi+\xi(\psi-2\beta^2)\}, \quad . \quad . \quad . \quad . \quad . \quad . \quad (21)$$

where
$$\phi=\beta(\coth\beta-\beta)+\rho^2\beta^3/(\beta-\tanh\beta) \quad . \quad . \quad . \quad (22)$$

and ψ is given by equation (16).

Consider now the shortening e of the strip, due to the change of slope. To the accuracy required this is given by

$$e=\int_0^L \tfrac{1}{2}\left(\frac{dy}{dx}\right)^2 dx=\frac{1}{2L}\int_0^1\left(\frac{dy}{dX}\right)^2 dX. \quad . \quad . \quad . \quad (23)$$

From equations (12) and (13)

$$\frac{dy}{dX}=\frac{L}{4\beta^2}\{2\beta m_A\sinh 2\beta X-f(\cosh 2\beta X-1)\}.$$

On substituting this expression into equation (23), performing the integration and substituting for m_A and f from (14) and (15), we obtain after considerable simplification,

$$e=\theta^2L\left[\frac{1}{16\beta}\{\beta(3-\coth^2\beta)+\coth\beta\}+\tfrac{1}{4}(\rho+\xi)+\right.$$
$$\left.+\frac{(\rho+\xi)^2\beta}{16(\beta-\tanh\beta)^2}\{3(\beta-\tanh\beta)-\beta\tanh^2\beta\}\right].$$

As pointed out previously, ξ is of order θ and, for the accuracy required, can be neglected in the above expression. Hence, writing $e=\lambda\theta^2 L$, we obtain finally

$$\lambda=\frac{1}{16\beta}\{\beta(3-\coth^2\beta)+\coth\beta\}+\tfrac{1}{4}\rho+$$
$$+\frac{\rho^2\beta}{16(\beta-\tanh\beta)^2}\{3(\beta-\tanh\beta)-\beta\tanh^2\beta\} \quad . \quad (24)$$

The forces in the strips have so far been derived in terms of

$$\beta=[PL^2/(4EI)]^{\frac{1}{2}}.$$

If the strip is in compression β becomes imaginary and for computation must be replaced by $i\gamma$ where

$$\gamma=[-PL^2/(4EI)]^{\frac{1}{2}}.$$

All the functions of β contained in equations (14) to (24) remain real and can be obtained by the substitutions $\beta=i\gamma$, $\sinh\beta=i\sin\gamma$ and $\cosh\beta=\cos\gamma$.

It will be seen from equation (19) that the bending moment then contains a term proportional to $\operatorname{cosec}\gamma$ which $\longrightarrow\infty$ as $\gamma\longrightarrow\pi$, when buckling of the strip occurs. This imposes an upper limit on the value of γ.

The limiting values of the various bending moments and the shear force as $\beta\longrightarrow 0$ are required. These are as follows:—

$$\left.\begin{aligned} m_A&=\theta\{1+3(\rho+\xi)\}\\ m_B&=\theta\{1-3(\rho+\xi)\}\\ f&=6\theta(\rho+\xi)\\ m&=\theta\{1+3(\rho+\xi)(1-2X)\}\\ m_O&=\theta\{1+3\rho(\rho+\xi)\}\end{aligned}\right\} \quad . \quad . \quad . \quad . \quad . \quad (25)$$

Also the shortening λ tends to the value

$$\lambda=\frac{1}{6}+\frac{1}{4}\rho+\frac{3}{20}\rho^2. \quad . \quad . \quad . \quad . \quad . \quad (26)$$

4. THE RELATION BETWEEN TORQUE AND ROTATION

A study of the preceding equations shows that the determination of exact values for the tensions in the strips when the pivot is in a displaced position would

involve the solution of a set of simultaneous equations, each one being of a complicated transcendental nature. The torque T is clearly a non-linear function of the rotation θ for given values of V and H and the relationship will be represented here by a power series in θ, thus

$$T=(EI/L)(K\theta+b\theta^2+\ldots) \quad . \quad . \quad . \quad . \quad . \quad (27)$$

where the coefficients K, b, . . . are functions of v and h.

Since terms in θ^2 have been retained, the equations so far derived are of a sufficiently high order of accuracy to determine the coefficients K and b in the series, but not the coefficients of the higher powers of θ.

The magnitudes of K and b will be determined from the fact that, for given values of v and h,

$$K=\frac{L}{EI}\left(\frac{dT}{d\theta}\right)_{\theta=0} \quad . \quad . \quad . \quad . \quad . \quad . \quad (28)$$

$$b=\frac{1}{2}\,\frac{L}{EI}\left(\frac{d^2T}{d\theta^2}\right)_{\theta=0} \quad . \quad . \quad . \quad . \quad . \quad . \quad (29)$$

Consider first the strip tensions when $\theta=0$. From equation (15) it will be seen that the shear forces in the strips are then zero so that, by virtue of equations (10),

$$\left.\begin{aligned}\beta_1^2&=\frac{1}{8}(v+h)\\ \beta_2^2&=\frac{1}{8}(v-h)\end{aligned}\right\} \quad . \quad . \quad . \quad . \quad . \quad . \quad (30)$$

and the two tensions are known.

Further, from equations (11) and (28),

$$K=\left\{\frac{dm_{o1}}{d\theta}+\frac{dm_{o2}}{d\theta}\right\}_{\theta=0} \quad . \quad . \quad . \quad . \quad . \quad (31)$$

Now, remembering that ξ is of the order of θ, equation (21) shows that

$$\left(\frac{dm_o}{d\theta}\right)_{\theta=0}=\phi.$$

Hence from (31),

$$K=\phi_1+\phi_2, \quad . \quad . \quad . \quad . \quad . \quad . \quad . \quad (32)$$

where ϕ_1 and ϕ_2 are the values of ϕ at $\beta=\beta_1$ and β_2 respectively, and β_1, β_2 are given by equations (30).

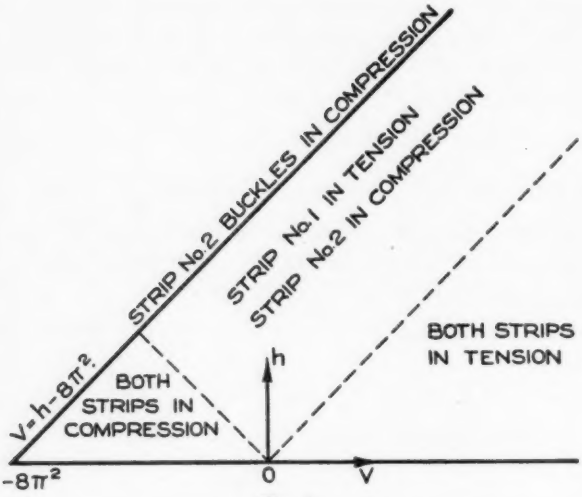

Fig. 5.
The working region in the v-h plane.

Let the value of K when $V=H=0$ be K_0. Then since $\beta_1=\beta_2=0$ from (30),

$$K_0=2\phi(0)=2(1+3\rho^2). \quad . \quad . \quad . \quad . \quad . \quad (33)$$

Considering positive values of h only, it will be seen from equations (30) that if $|v|>h$ both strips are in tension or both in compression according to the sign of v. If $|v|<h$ one strip is in tension and one in compression. Further, one strip buckles in compression when v reaches the value $(h-8\pi^2)$. These considerations lead to Fig. 5 which shows the region in the v-h plane in which possible values of v and h must lie. It also shows whether the strips are in tension or compression. (Note that in Fig. 3, the strip No. 1 is the strip in which the side force H is inducing tension.)

Equations (30) enable a chart to be constructed showing the values of β_1^2 and β_2^2 for a range of values of v and h within the region of Fig. 5. The values of ϕ_1 and ϕ_2 then follow from equation (22) and the stiffness K from (32). This has been done for three pivots in which $\rho=0$, ± 1 and $\pm\sqrt{5}/3$ $(=0.745)$, and the results, given in the form K/K_0, are shown graphically in Figs. 6, 7 and 8 respectively.

In each of these diagrams the upper curve corresponds to $H=0$ so that the application of a side force always reduces the stiffness of a pivot. From Fig. 6 it will be seen that a pivot in which the strips cross at their middle points $(\rho=0)$ rapidly becomes unstable (*i.e.* the stiffness K becomes negative) when a vertical tensile force is applied. With a vertical compressive force the stiffness K rises to a

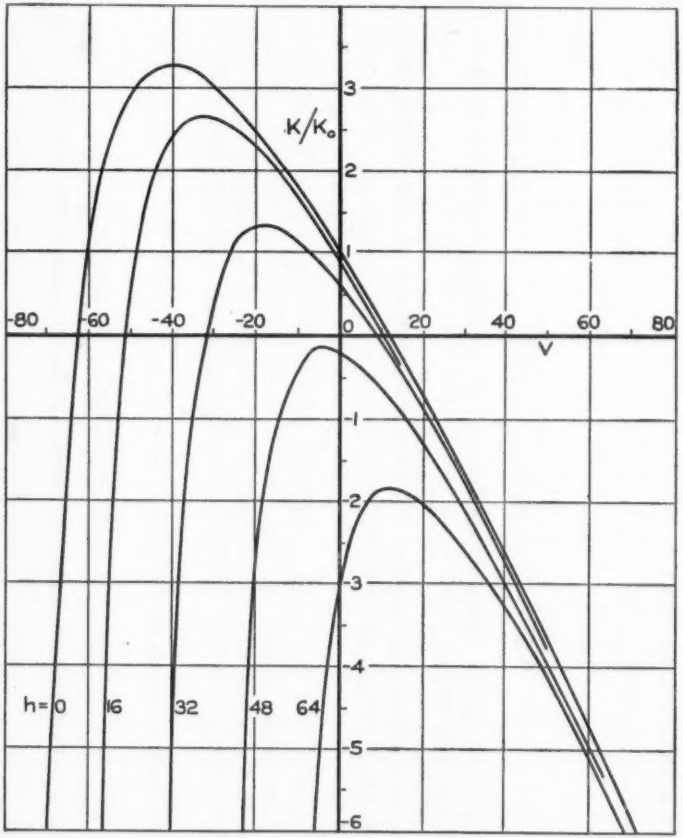

Fig. 6.
Stiffness diagram – $\rho = 0$ ($K_0 = 2$).

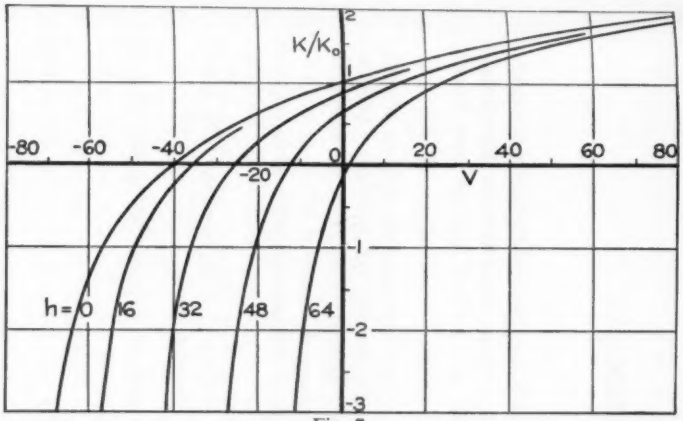

Fig. 7.
Stiffness diagram – $|\rho| = 1$ ($K_0 = 8$).

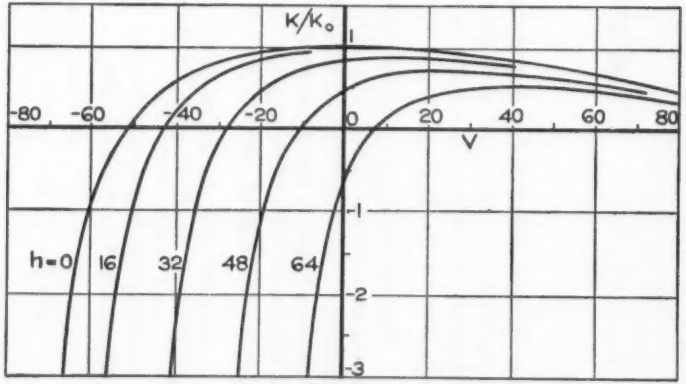

Fig. 8.
Stiffness diagram – $|\rho| = \sqrt{5}/3 = 0.745$ ($K_0 = 16/3$).

maximum of about $3.25K_0$ (occurring at $v=-40$) and then rapidly becomes negative as strip No. 2 approaches its buckling load. These characteristics are changed completely by crossing the strips at one end ($\rho=\pm 1$), as will be seen from a consideration of Fig. 7.

The application of a vertical tensile force then increases the stiffness whereas a compressive force decreases it. If $h<62$ approximately, the pivot never becomes unstable when v is positive. The intermediate value of $\rho=\pm\sqrt{5/3}$, the results for which are shown in Fig. 8, has been chosen because the value of $\partial K/\partial v$ at $v=h=0$ is then zero. This pivot may be useful when a constant value for K is required over a small range of vertical force.

Consider now the determination of the coefficient b in equation (27), giving a measure of the non-linearity of the torque-rotation curve.

First differentiate equation (15) with respect to θ, remembering that ξ is of order θ, and then put $\theta=0$, thus

$$\left(\frac{df}{d\theta}\right)_{\theta=0}=2\psi. \quad . \quad . \quad . \quad . \quad . \quad . \quad . \quad (34)$$

Now differentiating equations (10) with respect to θ, keeping v and h constant, and then putting $\theta=0$, we obtain

$$\left.\begin{aligned}\left(\frac{d\beta_1}{d\theta}\right)_{\theta=0}&=\frac{1}{4\beta_1}(\psi_1\cot 2\alpha+\psi_2\operatorname{cosec}2\alpha)\\ \left(\frac{d\beta_2}{d\theta}\right)_{\theta=0}&=-\frac{1}{4\beta_2}(\psi_2\cot 2\alpha+\psi_1\operatorname{cosec}2\alpha)\end{aligned}\right\} \quad . \quad . \quad . \quad (35)$$

where ψ_1, ψ_2 are the values of ψ at $\beta=\beta_1$ and β_2 respectively, and β_1, β_2 are given by equations (30).

Next differentiate equation (21) twice with respect to θ, remembering again that ξ is of order θ, and then put $\theta=0$, thus

$$\left(\frac{d^2m_o}{d\theta^2}\right)_{\theta=0}=\left\{2\phi'\frac{d\beta}{d\theta}+2\frac{\xi}{\theta}(\psi-2\beta^2)\right\}_{\theta=0}, \quad . \quad . \quad . \quad (36)$$

where $$\phi'=\frac{d\phi}{d\beta}=\coth\beta-\beta(\coth^2\beta+1)+\rho^2\beta^2\left\{\frac{3}{\beta-\tanh\beta}-\frac{\beta\tanh^2\beta}{(\beta-\tanh\beta)^2}\right\}. \quad (37)$$

Now, from equations (6) and (17),

$$\left.\begin{aligned}\xi_1/\theta&=\tfrac{1}{2}(1+\rho)\tan\alpha+2\lambda_1\cot 2\alpha-2\lambda_2\operatorname{cosec}2\alpha\\ -\xi_2/\theta&=\tfrac{1}{2}(1+\rho)\tan\alpha+2\lambda_2\cot 2\alpha-2\lambda_1\operatorname{cosec}2\alpha\end{aligned}\right\} \quad . \quad . \quad (38)$$

Hence, substituting (11) and (36) into (29) and using equations (35) and (38) we obtain finally

$$b=\left\{\frac{\phi_1'}{\beta_1}(\psi_1\cos 2\alpha+\psi_2)-\frac{\phi_2'}{\beta_2}(\psi_2\cos 2\alpha+\psi_1)\right\}(\operatorname{cosec}2\alpha)/4+$$
$$+(\psi_1-2\beta_1^2)\{\tfrac{1}{2}(1+\rho)\tan\alpha+2\lambda_1\cot 2\alpha-2\lambda_2\operatorname{cosec}2\alpha\}-$$
$$-(\psi_2-2\beta_2^2)\{\tfrac{1}{2}(1+\rho)\tan\alpha+2\lambda_2\cot 2\alpha-2\lambda_1\operatorname{cosec}2\alpha\}. \quad (39)$$

For given values of v and h, the values of β_1 and β_2 are obtained from equations (30), then ϕ_1' and ϕ_2' from (37), ψ_1 and ψ_2 from (16), λ_1 and λ_2 from (24), and the value of b then follows from (39).

If the side force H is zero, equations (30) give $\beta_1=\beta_2$ so that $\phi_1'=\phi_2'$, $\psi_1=\psi_2$ and $\lambda_1=\lambda_2$ and equation (39) then gives $b=0$. This result could have been obtained simply by a consideration of the symmetry of the pivot since if the side force is zero the torque T must be an odd function of the rotation θ. Consequently it is to be expected that the relation between the torque and rotation will be much more non-linear in the presence of a side force than with no such force acting.

In the particular case of a pivot in which the strips cross at right angles ($\alpha=45°$) equation (39) reduces to

$$b=\frac{\phi_1'\psi_2}{4\beta_1}-\frac{\phi_2'\psi_1}{4\beta_2}+(\psi_1-2\beta_1^2)\{\tfrac{1}{2}(1+\rho)-2\lambda_2\}-(\psi_2-2\beta_2^2)\{\tfrac{1}{2}(1+\rho)-2\lambda_1\}$$
. . . (40)

5. THE WORK DONE IN DISPLACING THE PIVOT

In considering the variations of rotational stiffness with applied load it is instructive to investigate the work done by the vertical and horizontal loads V and H and by the torque T during a small rotation θ. For this purpose the horizontal and vertical movements of the point G (Fig. 2) are required in the directions of H and V respectively. Neglecting terms in θ^3 these may be shown to be $\frac{1}{2}(\lambda_2-\lambda_1)\theta^2L\operatorname{cosec}\alpha$ and $\{\frac{1}{2}(1+\rho)-\frac{1}{2}(\lambda_1+\lambda_2)\}\theta^2L\sec\alpha$ respectively.

It should be noticed that if $h=0$ so that $\beta_1=\beta_2=\beta$ say and $\lambda_1=\lambda_2=\lambda$ say, the horizontal movement of G is zero and the vertical movement is $\frac{1}{4}(1+\rho-4\lambda)\theta^2L\sec\alpha$. If in addition $v=0$ so that $\beta=0$, the shortening λ is given by (26) and the vertical movement of G then becomes

$$\frac{1}{60}(5-9\rho^2)\theta^2L\sec\alpha.$$

This is zero if $\rho=\pm\sqrt{5}/3$ so that in this case the point G coincides with O to a high order of accuracy. If $|\rho|<\sqrt{5}/3$ the point G moves downwards (*i.e.* in the

direction of V) whereas if $|\rho| > \sqrt{5}/3$ the point G moves upwards. This explains the different types of stiffness variation shown in Figs. 6, 7 and 8.

The work done by the forces V and H is given by

$$W_V + W_H = \theta^2 L [\{ \tfrac{1}{4}(1+\rho) - \tfrac{1}{2}(\lambda_1 + \lambda_2) \} V \sec\alpha + \tfrac{1}{2}(\lambda_2 - \lambda_1) H \operatorname{cosec}\alpha].$$

Using equations (9) and (10) and neglecting terms in θ^3 this becomes

$$W_V + W_H = \frac{EI\theta^2}{L} \{ \beta_1^2 (1+\rho-4\lambda_1) + \beta_2^2 (1+\rho-4\lambda_2) \}.$$

Further, neglecting terms in θ^3, the work done by the torque is given by

$$W_T = \tfrac{1}{2}\theta T = (EI\theta^2/L)(\tfrac{1}{2}\phi_1 + \tfrac{1}{2}\phi_2).$$

The strain energy U stored in a strip is

$$U = \frac{EI}{2L} \int_0^1 m^2 dX.$$

On substituting (19), performing the integration and neglecting terms in θ^3, this gives after considerable simplification,

$$U = \frac{EI\theta^2}{L} \{ \beta^2 (1+\rho-4\lambda) + \tfrac{1}{2}\phi \},$$

where ϕ and λ are the functions of β given in equations (22) and (24). Hence

$$W_V + W_H + W_T = U_1 + U_2,$$

giving a check on the preceding analysis.

It should be emphasised that the point G is not the instantaneous centre of rotation of the displaced pivot but merely the displaced position of the initial centre. The actual instantaneous centre lies at a point whose horizontal and vertical distances from O in the directions of H and V are equal to $\{ (\lambda_2 + \lambda_1) - \tfrac{1}{2}(1+\rho) \} \theta L \sec\alpha$ and $(\lambda_2 - \lambda_1)\theta L \operatorname{cosec}\alpha$ respectively, where terms of order θ^2 have been neglected. If $\rho = \pm\sqrt{5}/3$ and $h = 0$ both these expressions are zero, so that for this particular pivot the distance between O and the instantaneous centre is of order θ^2, and therefore the centre of rotation is fixed to a higher order of accuracy than in other pivots.

6. THE GREATEST STRESSES IN THE STRIPS

In designing a pivot the maximum stress in each strip, for given values of v, h and θ, is required. For this purpose the second order terms which have so far

been retained in the analysis can be discarded. This amounts to putting $\xi=0$ in equations (14) to (21), so that the terminal bending moments are then given by

$$m_{A,B}=\theta\left\{\beta\coth\beta\pm\rho\frac{\beta^2\tanh\beta}{\beta-\tanh\beta}\right\} \quad . \quad . \quad . \quad . \quad (41)$$

and the bending moment m at any point in the strip becomes

$$m=\theta\left\{\beta\,\mathrm{cosech}\,\beta\cosh\beta(1-2X)+\rho\frac{\beta^2\,\mathrm{sech}\,\beta}{\beta-\tanh\beta}\sinh\beta(1-2X)\right\}. \quad (42)$$

The shear force f is given simply by

$$f=2\theta\psi.. \quad . \quad . \quad . \quad . \quad . \quad . \quad (43)$$

The tensions in the strips may be assumed independent of the rotation for design purposes so that β_1 and β_2 are then given by equations (30).

In each strip the stress at any point is the algebraic sum of the uniform stress due to the tension and the stress due to the bending moment m. The maximum stress therefore occurs where the bending moment has its greatest numerical value. Because of the difference in behaviour of the hyperbolic functions which arise when β is real and the trigonometric functions when β is imaginary, the tension and compression cases must be considered separately in determining the greatest bending moment.

(*a*) *The strip in tension* (β *real*)

Consider first the case of $\rho>0$.

If the tension is zero ($\beta=0$) equations (25) with $\xi=0$ give

$$m_A=\theta(1+3\rho),\ m_B=\theta(1-3\rho),\ m=\theta(1+3\rho-6\rho X).$$

Hence in this case $|m_A|>|m_B|$, and the variation of m with x is linear. The greatest bending moment is then equal to m_A.

Further, since $\beta\coth\beta>0$ and $\beta^2\tanh\beta/(\beta-\tanh\beta)>0$, it is clear from equation (41) that $|m_A|>|m_B|$ for all real values of β. This does not necessarily mean that m_A is always the greatest bending moment, since for non-zero values of β the variation of m with x is not linear. There is therefore the possibility of a stationary value of m occurring inside the strip for some values of β. If this does occur, however, it is clear from equation (18) that the magnitude of the stationary bending moment, m_s say, is given by

$$m_s^2=m_A^2-\left(\frac{f}{2\beta}\right)^2.$$

This shows that $|m_A| > |m_s|$ and it is concluded therefore that if $\rho > 0$ the greatest bending moment is m_A, occurring at the fixed end, for all values of β. An exactly similar argument shows that if $\rho < 0$ the greatest bending moment is m_B, occurring at the moving end. It will be seen from equation (41) that both possibilities may be combined in one expression for the greatest bending moment, m_{max}, by replacing $\pm\rho$ by $|\rho|$, thus

$$m_{max} = \theta \left\{ \beta \coth \beta + |\rho| \frac{\beta^2 \tanh \beta}{\beta - \tanh \beta} \right\} \quad . \quad . \quad . \quad (44)$$

(*b*) *The strip in compression* (γ *real*)

Substitution of $\beta = i\gamma$ in equations (41) and (42) yields

$$m_{A,B} = \theta \left\{ \gamma \cot \gamma \pm \rho \frac{\gamma^2 \tan \gamma}{\tan \gamma - \gamma} \right\} \quad . \quad . \quad . \quad . \quad (45)$$

$$m = \theta \left\{ \gamma \operatorname{cosec} \gamma \cos \gamma (1 - 2X) + \rho \frac{\gamma^2 \sec \gamma}{\tan \gamma - \gamma} \sin \gamma (1 - 2X) \right\} \quad . \quad (46)$$

Consider first the case of $\rho > 0$.

As before, if the compression is zero, $|m_A| > |m_B|$ and the variation of m with x is linear so that m_A is the greatest bending moment.

Also, from (45), $$m_A^2 - m_B^2 = 4\rho\theta^2 \frac{\gamma^3}{\tan \gamma - \gamma}.$$

Hence, if $0 < \gamma < \pi/2$, $|m_A| > |m_B|$

and if $\pi/2 < \gamma < \pi$, $|m_B| > |m_A|$.

The possibility of a stationary value of m occurring at some point in the strip must now be investigated. If this happens its value m_s may be obtained from either equation (18) or (46), thus

$$m_s^2 = m_A^2 + \left(\frac{f}{2\gamma}\right)^2 \quad . \quad . \quad . \quad . \quad . \quad . \quad . \quad . \quad (47)$$

$$= \theta^2 \left\{ \gamma^2 \operatorname{cosec}^2 \gamma + \rho^2 \frac{\gamma^4 \sec^2 \gamma}{(\tan \gamma - \gamma)^2} \right\} \quad . \quad . \quad . \quad . \quad (48)$$

Using equations (45) and (48) we obtain, after some reduction,

$$m_s^2 = m_B^2 + \theta^2 \left\{ \gamma + \rho \frac{\gamma^2}{\tan \gamma - \gamma} \right\}^2 \quad . \quad . \quad . \quad . \quad . \quad (49)$$

Equations (47) and (49) show that if a stationary value does occur, it will be numerically greater than either of the terminal bending moments and therefore will be the greatest bending moment in the strip.

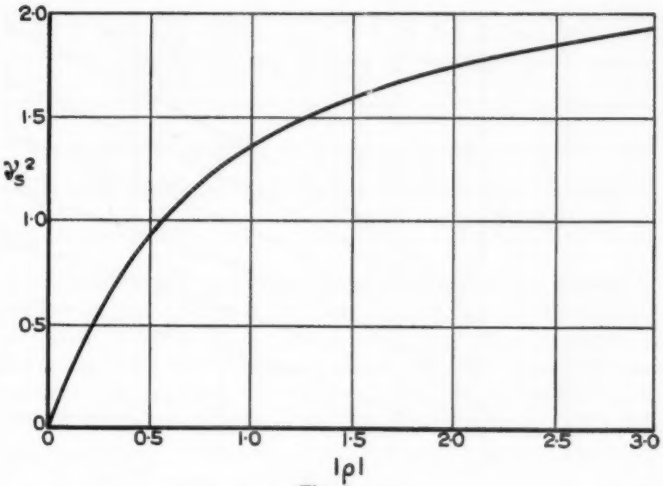

Fig. 9.
Variation of γ_s^2 with $|\rho|$.

It remains to find at what value of γ it first occurs. This is clearly the value at which dm/dX first becomes zero at one or other of the two ends of the strip.

From (18), $dm/dX=0$ at $X=0$ when $f=0$. By virtue of equations (43) and (16) this gives

$$\tan\gamma=(1+\rho)\gamma. \quad . \quad . \quad . \quad . \quad . \quad . \quad (50)$$

If $\rho>0$ this equation has a root, γ_s say, in the range $0<\gamma<\pi/2$ and for $\gamma>\gamma_s$ a stationary value of m will occur inside the strip.

Also, from equation (46), $dm/dX=0$ at $X=1$ when

$$\tan\gamma=(1-\rho)\gamma. \quad . \quad . \quad . \quad . \quad . \quad . \quad (51)$$

This equation has no root in the range $0<\gamma<\pi$ if $0<\rho<1$. If $\rho>1$ a root occurs in the range $\pi/2<\gamma<\pi$, but this is clearly greater than γ_s, the root of equation (50), so that the stationary value of m_s first occurs at $\gamma=\gamma_s$.

To summarise, it has been shown that if $0<\gamma<\gamma_s$ the greatest bending moment is m_A occurring at the fixed end, while if $\gamma>\gamma_s$ the greatest bending moment is m_s occurring at some point inside the strip.

An exactly similar argument applies if $\rho<0$, in which case the greatest bending moment is m_B if γ is less than the lowest root of equation (51). If γ is greater than this value the greatest bending moment is m_s.

As in the tension case the two possibilities of positive and negative ρ may be combined to give the following:

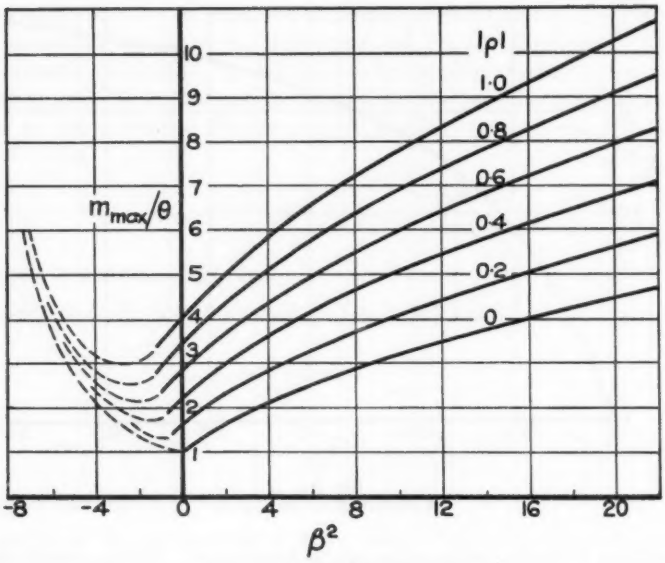

Fig. 10.
Maximum bending moment in a strip.

(*i*) if $0<\gamma<\gamma_s$, where γ_s is the lowest root of the equation $\tan\gamma=(1+|\rho|)\gamma$, the greatest bending moment occurs at one end of the strip and has the value

$$m_{max}=\theta\left\{\gamma\cot\gamma+|\rho|\frac{\gamma^2\tan\gamma}{\tan\gamma-\gamma}\right\} \quad . \quad . \quad . \quad . \quad (52)$$

(*ii*) if $\gamma>\gamma_s$ the greatest bending moment occurs at some point inside the strip, its value being m_s given by equation (48).

The variation of γ_s^2 with $|\rho|$ is shown graphically in Fig. 9. Also, the preceding results have been used to draw the curves of Fig. 10 which show the variation of m_{max}/θ in a strip with the tension (β^2) for six positions of the point at which the strips cross, ranging from $\rho=0$ to $|\rho|=1$. In each curve the full line portion indicates that the maximum bending moment occurs at one end while over the dotted portion the maximum bending moment occurs somewhere inside the strip.

REFERENCES

1. WITTRICK, W. H. (1948). The Theory of Symmetrical Crossed Flexure Pivots. *Aust. J. Sci. Res.*, A, Vol. 1, No. 2, pp. 121-134, 1948.

2. HARINGX, J. A. (1949). The Cross-Spring Pivot as a Constructional Element. *App. Sci. Res.*, A, Vol. 1, No. 4, pp. 313-332, 1949.

AN ANALYSIS OF THE LIFT ON STRAIGHT, YAWED AND SWEPT-BACK WINGS

by

J. LOCKWOOD TAYLOR, D.Sc., M.I.N.A.
(formerly Professor of Aeronautics, The Technical University, Istanbul)

SUMMARY

As is well known, standard lifting-line theory cannot be applied to a wing with sweepback in order to determine the amount and distribution of the lift. Various methods, all fairly laborious, are available, and while they give results which agree fairly well with experiment, they do not show in detail the source of the various differences due to sweep. It is with the object of separating the several effects involved, which can be regarded as distinct for practical purposes, that the present method has been developed. Since one of the items, finite-chord loss, is shared with the straight wing, although not included in simple lifting-line theory, it is calculated first for the straight wing. The wing is represented by its median or camber surface and is assumed nearly flat.

The various effects may be summarised as follows:—

(*i*) Finite-chord effect; the reduction in lift for finite-chord (or aspect ratio) over and above that given by lifting-line theory.

(*ii*) (*a*) Cosine effect at infinite aspect ratio; according to this the lift is reduced in the ratio $\cos\lambda$, where λ is the angle of sweep.
(*b*) Modification of (*a*) for finite aspect ratio applying approximately to either yawed or swept wings.

(*iii*) The gain in lift at either wing tip, approximately equal to that for the rear tip of a yawed wing.

(*iv*) The effect of the central kink in the plan form.

Notation

w	downwash velocity
w_0	downwash velocity, lifting-line theory
U	aircraft velocity
K	circulation constant
K'	strength of element of circulation

Paper received January 1950.
[The Aeronautical Quarterly, Vol. II, February 1951]

x	co-ordinate measured downstream from origin of vortex
y	co-ordinate measured crosswind from origin of vortex
x_1, y_1, x_2, y_2	co-ordinates measured perpendicular and parallel to yaw or sweep respectively
r^2	$=x^2+y^2$, $r_1^2=(x+c)^2+y^2$, $r_2^2=(x-c)^2+y^2$, $r'^2=(y\tan\lambda+2c)^2+y^2$
λ	angle of yaw or sweep
c	semi-chord
s	semi-span
n	$=1, 2, 3 \ldots$
A_n	a constant
θ, ϕ	specified by $s\cos\theta$ or $s\cos\phi$ = distance from centre line to wing station
I, I'	integrals
C_L	lift coefficient
α	angle of incidence
a_0	lift-slope $dC_L/d\alpha$, infinite aspect ratio
c.p.	centre of pressure
A.R.	aspect ratio

1. STRAIGHT WING FINITE-CHORD EFFECT

The estimation of the effect of finite-chord (for a straight wing) is made by calculating the downwash at the ¾ chord by an analytical method based on an exact solution for a uniformly-loaded rectangular wing. The derivation of this solution is being published elsewhere but will be summarised briefly. A single element of a wing vortex system of strength K' comprising bound and trailing vortices, gives a downwash

$$\frac{w}{U}=\frac{K'}{4\pi}\left(\frac{y}{xr}+\frac{x}{yr}+\frac{1}{y}\right)$$

the origin of co-ordinates, $x=y=0$ being at the intersection of the two vortex lines; x is positive downstream and $r^2=x^2+y^2$.

The second and third terms of the downwash represent the trailing vortex and the first the bound vortex. The combined vortex is anti-symmetrical in y and Tee-shaped, the vorticity at the x-axis being of opposite sign on the two sides of the y-axis. If to the first term is added a term $1/x$, this annuls the vorticity at the axis of x for y negative and transforms the T vortex into a right angle (Γ). This can be regarded as the departure from two-dimensional flow round the aerofoil for negative values of y. Similarly, addition of $-1/x$ gives the departure for positive y,

converting the T into ⅂ (y positive to the right). For uniform chordwise loading over a wing of chord $2c$

$$\frac{w}{U} = \frac{K'}{4\pi}\int_{x-c}^{x+c}\left(\frac{y}{xr} - \frac{1}{x} + \frac{x}{yr} + \frac{1}{y}\right)dx \qquad (y \text{ positive})$$

$$= \frac{K'}{4\pi}\left[-\log(r+y) + \frac{r}{y} + \frac{x}{y}\right]_{x=x-c}^{x=x+c}$$

$$= \frac{K'}{4\pi}\left\{\log\left(\frac{r_2+y}{r_1+y}\right) + \frac{r_1-r_2}{y} + \frac{2c}{y}\right\}$$

where $r_1 = \{(x+c)^2+y^2\}^{\frac{1}{2}}$

$r_2 = \{(x-c)^2+y^2\}^{\frac{1}{2}}$.

The final term is the trailing-vortex downwash as used in lifting-line theory, the second term is the gradient of the trailing-vortex downwash, and the first term is due to the termination of the bound vortex.

Numerical evaluation (*see* Appendix) shows that both the first two terms, representing the departure from lifting-line theory, can be represented with fair approximation, in terms suitable for integration, as follows,

trailing-vortex term	$\frac{4x}{c}\frac{c}{y}\left(\frac{1}{1+2y/c}\right)\frac{K'}{4\pi}$
bound-vortex term	$-\frac{2x}{c}\frac{c}{y}\left(\frac{1}{1+2y/c}\right)\frac{K'}{4\pi}$
net downwash correction	$\frac{2x}{c}\frac{c}{y}\left(\frac{1}{1+2y/c}\right)\frac{K'}{4\pi}$

The range of validity of the approximation to the net correction is $x/y \gg 1.5$ say, and for moderately small values of y, $x \gg c$.

Only the net correction is required in the present application to a straight wing but the separate terms will be needed in dealing with yawed wings. Expressed as a fraction of the lifting-line downwash, the net correction is $(x/c)/(1+2y/c)$ and if we assume this is independent of the chordwise distribution, provided x is measured from the centre of pressure (this has been checked by independent calculation for a parabolic chordwise loading (*see* Appendix) giving c.p.$=0.25$) and take $x=c$ so as to give the downwash at the ¾ chord (if the c.p. is as usual at 0.25), the integrals corresponding with $2c/[y(1+2y/c)]$ or $2c/y - 4/(1+2y/c)$ must be evaluated. The first integral is the usual lifting-line integral, namely, if

$K=4sU\Sigma A_n \sin n\theta$ in the usual notation,

$$\frac{w_0}{U}=\frac{1}{\pi}\int_0^{\pi}\frac{\Sigma nA_n\cos n\theta}{\cos\theta-\cos\phi}\,d\theta=\Sigma nA_n\frac{\sin n\phi}{\sin\phi}$$

The second integral is

$$I+I'=\frac{1}{\pi}\int_0^{\phi}\frac{\Sigma nA_n\cos n\theta}{c/2s+(\cos\theta-\cos\phi)}\,d\theta+\frac{1}{\pi}\int_{\phi}^{\pi}\frac{\Sigma nA_n\cos n\theta}{-c/2s+(\cos\theta-\cos\phi)}\,d\theta$$

$$=\Sigma nA_nI_n+\Sigma nA_nI'_n,$$

the splitting into two parts being necessary in order to take care of the discontinuity at $y=0$ (or $\theta=\phi$) already noted. The integrals can be evaluated without difficulty, and Table I gives, as an example, values for A.R.6, $c/(2s)=1/12$.

The suffixes in Table I refer to n, the coefficient of θ in the series. Odd values only are required in symmetrical-load problems.

$I_{(180-\phi)}=I'_{(\phi)}$ (n odd) and $I_{(180-\phi)}=-I'_{(\phi)}$ (n even) gives the values for the other semi-span, required for the yaw case.

The corrected downwash

$$\frac{w}{U}=\frac{2w_0}{U}-\Sigma(I_n+I'_n)nA_n.$$

TABLE I

ϕ	0	30°	45°	60°	90°
I_0	0	1.037	1.055	1.030	1.015
I'_0	−2.4	−2.37	−1.223	−1.108	−1.015
I_1	0	0.979	0.906	0.762	0.4155
I'_1	−1.6	−1.415	−0.216	0.020	0.4155
I_2	—	0.812	—	0.157	−0.448
I'_2	—	−0.631	—	0.58	0.448
I_3	0	0.569	0.069	−0.356	−0.34
I'_3	−0.711	−0.062	0.581	0.381	−0.34
I_4	—	0.29	—	−0.454	0.294
I'_4	—	0.304	—	−0.135	−0.294
I_5	0	−0.03	−0.435	−0.159	0.29
I'_5	−0.316	0.50	−0.05	−0.39	0.29

Hence equations corresponding with those of Glauert for the lifting-line can be written down by virtue of the relation

$$\left(\alpha - \frac{w}{U}\right) a_0 cU = K = 4sU \Sigma A_n \sin n\theta.$$

For the particular case of the rectangular wing of A.R.6, taking $a_0 = 2\pi$, we find, taking three terms of the series and using the 0, 45°, 90° stations,

$$A_1 = 0.226 \qquad A_3 = 0.014 \qquad A_5 = -0.0018 \qquad (\alpha = 1)$$

or taking 30°, 60°, 90°,

$$A_1 = 0.2155 \qquad A_3 = 0.006 \qquad A_5 = -0.0023.$$

It seems reasonable to take the mean values

$$A_1 = 0.221 \qquad A_3 = 0.010 \qquad A_5 = -0.002.$$

The convergence is very satisfactory and considerably better than for lifting-line theory. The lift-slope is $\pi s A_1/c = 0.663 \times 2\pi$, as compared with Glauert's value $0.72a_0$, a decrease of nearly 8 per cent. Figures in Ref. 1 from various sources range from 5 to 8 per cent. for similar aspect ratios, and there is experimental confirmation from two-dimensional tunnel results.

It is of interest to note that the loading is nearly elliptic, even for the rectangular wing when the corrected downwash at the $\frac{3}{4}$ chord is taken. The c.p. shift can be obtained by comparing the downwash w_0 at $\frac{1}{4}$ chord (or assumed c.p.) and at $\frac{3}{4}$ chord, and hence evaluating the induced camber. It is found that the shift is small except at the tip, the mean being 0.01 chord giving c.p. = 0.24 corrected. The induced drag, since it depends on the vortex wake at a distance (*i.e.* K) will be very nearly as for elliptic loading in spite of the appreciable increase in incidence for a given lift.

2. YAW EFFECT

(*a*) The reduction of lift in the ratio $\cos\lambda$ for an infinite-span constant-section yawed wing follows from resolution of the velocity U into components $U\cos\lambda$ and $U\sin\lambda$ normal and parallel to the wing generators. The incidence, camber ratio and zero-lift angle are all increased in the ratio $\sec\lambda$ for a normal section as compared with one parallel to U so that the lift is reduced as $\cos\lambda$ at any given fore-and-aft incidence. A similar result is obtained by considering the downwash, remote from the trailing vortex, due to a bound vortex strength $K\cos\lambda$ distributed over the normal chord $2c\cos\lambda$. The vertical velocity component at any point in the chord is as for vorticity K distributed over chord $2c$, as required.

(*b*) At finite aspect ratio there will be a correction to the $\cos\lambda$ factor. This has been estimated for a 30° yawed uniform-chord untwisted wing of aspect ratio 6

(the wing tips are streamwise) by substituting $(\alpha - w/U)\cos\lambda$ for $\alpha - w/U$ in the fundamental equation and allowing for sweep in the calculation of w for given K as follows. Using the same approximation as before for the trailing vortex field, but writing $x/c = 1 - (y\tan\lambda)/c$ to allow for sweep or yaw angle λ,

$$\frac{w}{U} = \frac{K'}{4\pi} 4\left(1 - \frac{y\tan\lambda}{c}\right)\left(\frac{c}{y} - \frac{2}{1+2y/c}\right) \qquad (y \text{ positive})$$

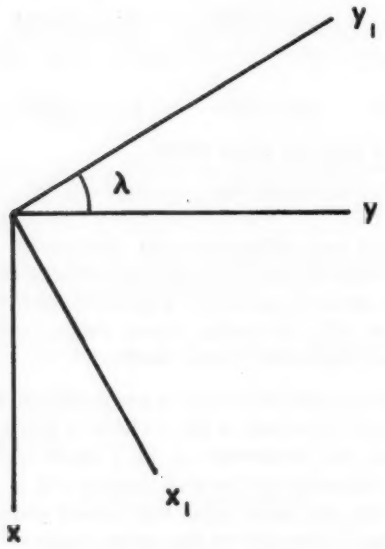

Fig. 1.
Yawed axes.

gives the downwash due to a trailing vortex element K' at c (half-chord) downstream from the centre of pressure line,

or $$\frac{w}{U} = \frac{K'}{4\pi} 4\left(\frac{c}{y} - \frac{2+\tan\lambda}{1+2y/c}\right). \qquad (y \text{ positive})$$

Similarly $$\frac{w}{U} = \frac{K'}{4\pi} 4\left(1 - \frac{y\tan\lambda}{c}\right)\left(\frac{c}{y} - \frac{2}{-1+2y/c}\right) \qquad (y \text{ negative})$$

$$= \frac{K'}{4\pi} 4\left(\frac{c}{y} - \frac{2-\tan\lambda}{-1+2y/c}\right).$$

The bound-vortex terms require separate treatment. Using co-ordinates y_1, x_1

parallel and perpendicular respectively to the sweep and therefore connected with y, x by the relations

$$y_1=(-x\sin\lambda+y\cos\lambda),\quad x_1=(x\cos\lambda+y\sin\lambda)\quad\text{(Fig. 1)},$$

the uniform-chordwise-load solution for the yawed wing is

$$\frac{w}{U}=\frac{K'}{4\pi}\int_{x-c}^{x+c}\left(\frac{y_1}{rx_1}-\frac{1}{x_1}\right)dx=\frac{-K'}{4\pi}\Big[\sec\lambda\log(r+y_1)+\tan\lambda\log(r+x)\Big]_{x=x-c}^{x=x+c}$$

$$=\frac{K'}{4\pi}\left\{\sec\lambda\log\left(\frac{r_2+y\cos\lambda-(x-c)\sin\lambda}{r_1+y\cos\lambda-(x+c)\sin\lambda}\right)+\tan\lambda\log\left(\frac{r_2+x-c}{r_1+x+c}\right)\right\}.$$

At the ¼ chord line, $x=c-y\tan\lambda$ is to be substituted; the resulting expression is given in the Appendix.

Numerical evaluation (*see* Appendix) gives as a working approximation

$$\frac{w}{U}=\frac{-K'}{4\pi}\frac{2c}{y}\left(\frac{1}{1+2y/c}\right)\sec\lambda=-\frac{K'}{4\pi}2\left(\frac{c}{y}-\frac{2}{1+2y/c}\right)\sec\lambda\quad(y\text{ positive})$$

i.e. as for the unyawed wing but with the additional factor $\sec\lambda$; there is a corresponding equation for y negative.

Collecting results for both bound and trailing vortex elements

$$\frac{w}{U}=\frac{K'}{4\pi}2\left\{\frac{(2-\sec\lambda)c}{y}-\frac{2(2+\tan\lambda-\sec\lambda)}{1+2y/c}\right\}\qquad(y\text{ positive})$$

$$\frac{w}{U}=\frac{K'}{4\pi}2\left\{\frac{(2-\sec\lambda)c}{y}-\frac{2(2+\tan\lambda-\sec\lambda)}{-1+2y/c}\right\}\qquad(y\text{ negative}).$$

The integrals to be evaluated are as before, apart from the constant factors depending on λ, the angle of yaw, namely

$$\frac{w}{U}=(3-\sec\lambda)\frac{w_0}{U}-(2+\tan\lambda-\sec\lambda)\Sigma I-(2-\tan\lambda-\sec\lambda)\Sigma I'.$$

Even values of n now occur in addition to odd values. Taking coefficients A_1 to A_5 inclusive and satisfying the downwash equation at $\phi=30°$, $60°$, $90°$, $120°$, $150°$ we get (for 30° yaw) $A_1=0.1969$, $A_2=0.0199$, $A_3=0.0119$, $A_4=0.0061$, $A_5=-0.0005$.

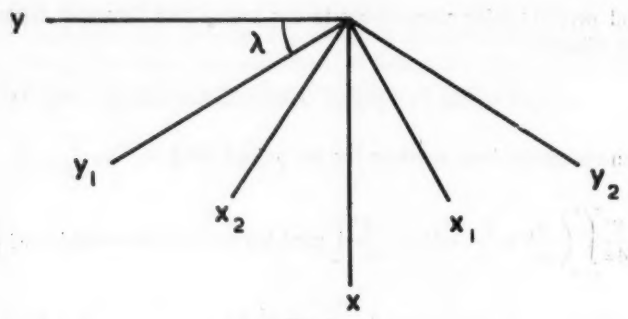

Fig. 2.
Central kink axes.

Comparing these values with those for the unyawed case, for which $A_1=0.221$, $A_3=0.010$, $A_5=-0.002$, the main difference in the symmetrical terms is a reduction in A_1 of about 11 per cent. to 0.89 of its original value, compared with 0.866 for $\cos\lambda$. The difference from infinite aspect ratio therefore is fairly small, and it seems reasonable to apply the result also to the swept wing of similar aspect ratio. The factor 0.89 compares with 0.85 given by Falkner[1] for an elliptic wing of aspect ratio 6.36 at 30° yaw.

3. TIP EFFECT

The results just calculated for a yawed straight wing include the local change of lift at the tips, namely decrease for the leading tip and increase for the rear tip. The fractional increase of lift on the rear semi-span is

$$[(2/3)A_2-(4/15)A_4]/[(\pi/4)A_1]=0.076.$$

That this is essentially a local effect can be shown by plotting the lift-grading (Fig. 3) and by evaluating the downwash due to the A_2, A_4 terms from the other semi-span, which is found to be negligible. Since this will apply equally to the swept as well as to the yawed wing it may be concluded that a similar increase of lift of 7.5 per cent. localised at the tip, will apply to each tip of a swept wing. The A_2 term also gives a value for the l_v derivative (rolling moment due to sideslip), namely $[(\pi s/4c)A_2/(\pi/6)]\lambda=0.18\lambda$ for the yawed wing. This is in fair agreement with other data (Ref. 3, p. 227) making allowance for some departure from linearity at the extreme sideslip angle of 30°.

4. KINK EFFECT

The central kink effect, again based on the exact result for uniform chordwise loading, may be evaluated by somewhat similar means. Considering a kinked

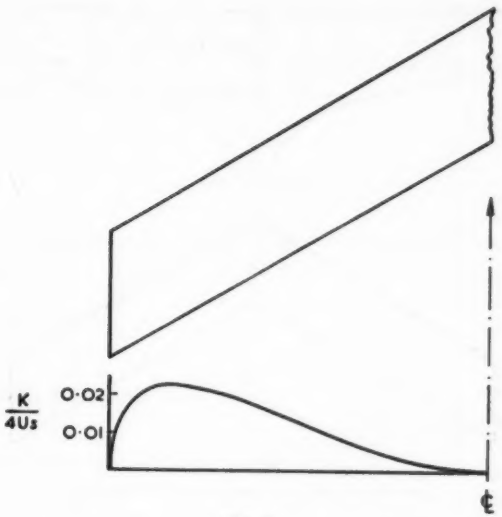

Fig. 3.
Local increase of lift at rear tip of 30° yawed wing, A.R.6.

straight-line vortex and taking axes (x_1, y_1) (x_2, y_2) with the y's along the respective vortex lines and the origin at their intersection so that

$$y_1 = x \sin\lambda + y \cos\lambda$$
$$x_1 = x \cos\lambda - y \sin\lambda$$
$$y_2 = x \sin\lambda - y \cos\lambda$$
$$x_2 = x \cos\lambda + y \sin\lambda,$$

(x, y are measured downwind and crosswind respectively (Fig. 2))

then
$$\frac{w}{U} = \frac{K}{4\pi}\left(\frac{y_1}{rx_1} - \frac{1}{x_1} + \frac{y_2}{rx_2} + \frac{1}{x_2}\right)$$

gives the downwash measured from the two-dimensional flow for the port half-wing, represented by $2/x_1$ as datum. Integrating as before

$$\int_{x-c}^{x+c} dx = \frac{K}{2\pi}\left[-\sec\lambda \log\left(\frac{x + r\sin\lambda}{rx_2}\right) + \tan\lambda \log(r+x)\right]_{x=x-c}^{x=x+c}$$

$$= \frac{K}{2\pi}\left\{\sec\lambda \log\frac{2r'\sin\lambda/(1+(c/y)\tan\lambda)}{(r'\sin\lambda + y\tan\lambda + 2c)} + \tan\lambda \log\frac{r' + y\tan\lambda + 2c}{y(\sec\lambda + \tan\lambda)}\right\}$$

where
$$r' = \{(y\tan\lambda + 2c)^2 + y^2\}^{\frac{1}{2}}.$$

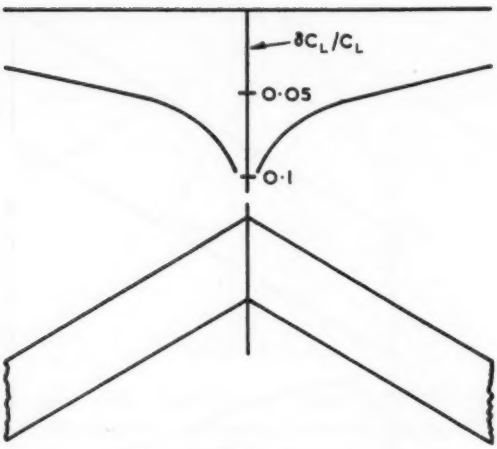

Fig. 4.
Loss of lift due to central kink (30° sweep).

Numerical evaluation gives the following results

A.R.	2	4	6
$\frac{2\pi\,(w/U)_{\text{mean}}}{K}$	0.40	0.34	0.28
$\delta C_L/C_L$	0.10	0.085	0.07

$2\pi w/U$ is equal to the reduction (δC_L) of C_L, due to the kink. Since the actual C_L at the centre line of the wing is $4K$, the fractional loss of lift, averaged over the span, is as given. The losses referred to the mean wing C_L are estimated as being 20 per cent. greater. Fig. 4 shows the spanwise distribution of $\delta C_L/C_L$ due to the kink.

Summing the various lift changes for a swept wing of A.R.6 compared with a straight wing

Due to cosine effect (Section 2(*a*))	− 11	per cent.
Due to wing tip effect (Section 3)	+ 7.5	per cent.
Due to central kink (Section 4)	− 8.5	per cent.
net	− 12	per cent.

Ref. 2 gives a lift loss of 14 per cent. for an elliptic wing of similar A.R. and there is some experimental confirmation from Ref. 4, pp. 394-5. If comparison is being made with straight-wing lifting-line theory the finite-chord loss (*i*) of about 8 per cent. must be added, giving 20 per cent. in all.

APPENDIX

Comparison of exact and approximate values of downwash correction

(i) Straight wing

Exact { Trailing-vortex correction $\frac{r_1 - r_2}{y}$; Bound-vortex correction $\log\left(\frac{r_2+y}{r_1+y}\right)$ } uniform chordwise loading.

Approximation to net correction, $\frac{2x}{c}\,\frac{c}{y}\left(\frac{1}{1+2y/c}\right)$

x/c (measured from c.p.)=		0.5	1.0	1.5	2.0	3.0
$y/c=0.5$	trailing vortex	1.74	3.12			
	bound vortex	0.56	0.94			
	net correction	1.18 (1.4)	2.18 (2.32)			
	approximation	1.0	2.0			
$y/c=1$	trailing vortex	0.68	1.24	1.57		
	bound vortex	0.28	0.47	0.56		
	net correction	0.40 (0.43)	0.77 (0.79)	1.01		
	approximation	0.33	0.67	1.0		
$y/c=2$	trailing vortex	0.22	0.415		0.68	
	bound vortex	0.10	0.19		0.28	
	net correction	0.12 (0.12)	0.225 (0.23)		0.40	
	approximation	0.10	0.20		0.40	
$y/c=3$	trailing vortex	0.103	0.20			0.47
	bound vortex	0.05	0.093			0.19
	net correction	0.053	0.107			0.28
	approximation	0.047	0.094			0.29

Figures in brackets are for parabolic chordwise loading.

(ii) Yawed or swept wing

The trailing-vortex correction has been taken as twice the approximation given for the net correction, which, as will be seen, limits the angle of sweep to rather less than 45°, $x/y=1$ approximately. The bound-vortex correction has been taken as $\sec\lambda\,\frac{2c}{y}\left(\frac{1}{1+2y/c}\right)$, the values of which are compared with the exact expression,

$$\sec\lambda \log\left\{\frac{\sqrt{[(2c-y\tan\lambda)^2+y^2]}-2c\sin\lambda+y\sec\lambda}{2y\sec\lambda}\right\}+$$

$$+\tan\lambda\log\left\{\frac{\sqrt{[(2c-y\tan\lambda)^2+y^2]}+2c-y\tan\lambda}{y(\sec\lambda-\tan\lambda)}\right\}$$

$y/c=$	0.5	1.0	2.0	4.0
Exact	1.41	0.65	0.22	0.045
Approximate	2.0	0.67	0.20	0.057

REFERENCES

1. FALKNER, V. M. (1943). Aerodynamic Loading on Surfaces of Any Shape. R. & M. 1910, August 1943.
2. COHEN, D. (1945). The Twist of a Surface for a Given Lift. N.A.C.A. Report 826, 1945.
3. CAMPBELL, J. P. (1948). Factors Affecting Lateral Stability. N.A.C.A. University Conference on Aerodynamics, June 1948.
4. RICHARDS, E. J. (1947). Practical Design Problems Arising from Sweepback. *Aeronautical Conference London*, 1947. Royal Aeronautical Society, 1948.

NOTICE TO CONTRIBUTORS

1. All communications should be addressed to the Secretary, Royal Aeronautical Society, 4 Hamilton Place, London, W.1.

2. Papers for consideration should be typewritten with double spacing and be accompanied by a summary of not more than 250-300 words.

3. Only simple symbols and formulae should be typewritten. All others should be written clearly in ink. Greek letters should be indicated and a clear distinction drawn between capital and small letters. Particular attention should be paid to the use of alpha and *a*, kappa and *k*, mu and *u*, nu and *v*, eta and *n*. The letter *l* must be distinguished from the numeral 1, and the letter *O* from the zero 0.

   The use of dots, bars, and so on, over letters or the use of dots as multiplication signs and bars for brackets should be avoided as far as possible.

   Suffixes and prefixes must be clearly indicated and complicated suffixes and prefixes should be avoided. The square root sign $\surd$ should be replaced by the index $\frac{1}{2}$.

4. A list of *all* symbols used *must* be given at the end of the paper whether they are standard or not.

5. *Clear* diagrams or sketches must be submitted for redrawing by the Society's draughtsman.

   Photographs must not be less than half plate size and must be clear black and white glossy prints.

6. References should be given in the form:—
   WARD, G. N. (1949). Calculation of Downwash Behind a Supersonic Wing. *The Aeronautical Quarterly*, Vol. I, May 1949, pp. 35-38.

7. The copyright of every paper printed in *The Aeronautical Quarterly* is the property of The Royal Aeronautical Society. Permission to reprint or to use any paper will not be unreasonably refused.

8. It is a condition of publication that the author shall have obtained consent where necessary to use any material in his paper which is copyright or the property of any other person or his employers.

9. Authors will be entitled to 25 reprints of their papers free of charge.

The Aeronautical Quarterly is published at the Offices of The Royal Aeronautical Society, 4 Hamilton Place, Piccadilly, London, W.1, at 10s. 0d. net for a single number to non-members and 7s. 6d. net for a single number to members of The Royal Aeronautical Society. Instructions for Contributors are given above. None of the papers must be taken as expressing the opinion of the Council of The Royal Aeronautical Society unless such is definitely stated to be the case. All communications for publication or advertisements in The Quarterly should be addressed to—The Secretary, J. Laurence Pritchard, 4 Hamilton Place, W.1.

Telephone: Grosvenor 3515 (5 lines). Telegraphic Address: Didaskalos, Audley, London.

THE AERONAUTICAL QUARTERLY

VOLUME II

PART I, MAY 1950

Two-Dimensional Theory of Stiffened Plates	*Chang O'Chou*
The Whirling of a Spinning Top	*J. Morris*
The Possibility of the Determination of Rate of Climb from Acceleration Measurements in Level Flight ...	*E. C. Pike*
A Note on Subsonic Aerofoil Theory	*John W. Miles*
Theory of an Oscillating Supersonic Aerofoil	*Geoffrey L. Sewell*
The Linearised Theory of Conical Fields in Supersonic Flow, with Applications to Plane Aerofoils ...	*S. Goldstein* and *G. N. Ward*

PART II, AUGUST 1950

Critical Mach Numbers for Swept-Back Wings ...	*S. Neumark*
General Performance Reduction Equations for Reciprocating-Engined Aircraft with Constant-Speed Propellers	*W. J. D. Annand*
The Axially-Symmetrical Supersonic Flow Near the Centre of an Expansion	*N. H. Johannesen* and *R. E. Meyer*
Note on the Dependence of Flap Hinge Moment Derivatives on Hinge Position	*W. J. Duncan*
On the Chordwise Lift Distribution at the Centre of Swept Wings	*D. Küchemann* and *J. Weber*
Erratum—(Volume I, Part IV) "A Note on the Bending Moment Induced in the Booms of a Spar at the point of Application of a Concentrated Load"	*H. F. Winny*

PART III, NOVEMBER 1950

Beams on Elastic Supports and on Cross Girders ...	*J. M. Klitchieff*
The Estimation of Range of Jet-Propelled Aircraft ...	*H. Pearson*
On Non-Steady Motion of Slender Bodies	*J. W. Miles*
The Correction of Wind Tunnel Nozzles for Two-Dimensional, Supersonic Flow	*R. E. Meyer* and *M. Holt*
Some Developments of Expansion Methods for Solving the Flutter Equations	*J. Williams*

Printed by the LEWES PRESS (Wightman & Co. Ltd.), Friars Walk, Lewes, England, and published by THE ROYAL AERONAUTICAL SOCIETY, 4 Hamilton Place, London, W.1, England.